

1 **The role of pre-existing structures during**
2 **rifting, continental breakup and transform**
3 **system development, offshore West Greenland**

4

5 Alexander L. Peace¹

6 Ken J. W. McCaffrey²

7 Jonathan Imber²

8 Jeroen van Hunen²

9 Richard Hobbs²

10 Woody Wilson³

11 ¹ Department of Earth Sciences, Memorial University of Newfoundland, St. John's, Newfoundland,
12 Canada

13 ² Department of Earth Sciences, Science Laboratories, Durham University, Durham, UK

14 ³ BP Exploration, Sunbury-on-Thames, Middlessex, UK

15 **Abstract**

16 Continental breakup between Greenland and North America produced the small
17 oceanic basins of the Labrador Sea and Baffin Bay, which are connected via the Davis
18 Strait, a region mostly comprised of continental crust. This study contributes to the
19 debate regarding the role of pre-existing structures on rift development in this region
20 using seismic reflection data from the Davis Strait data to produce a series of seismic
21 surfaces, isochrons and a new offshore fault map from which three normal fault sets
22 were identified as (i) NE-SW, (ii) NNW-SSE and (iii) NW-SE. These results were
23 then integrated with plate reconstructions and onshore structural data allowing us to
24 build a two-stage conceptual model for the offshore fault evolution in which basin
25 formation was primarily controlled by rejuvenation of various types of pre-existing

26 structures. During the first phase of rifting between at least Chron 27 (ca. 62 Ma;
27 Palaeocene), but potentially earlier, and Chron 24 (ca. 54 Ma; Eocene) faulting was
28 primarily controlled by pre-existing structures with oblique normal reactivation of
29 both the NE-SW and NW-SE structural sets in addition to possible normal
30 reactivation of the NNW-SSE structural set. In the second rifting stage between Chron
31 24 (ca. 54 Ma; Eocene) and Chron 13 (ca. 35 Ma; Oligocene), the sinistral Ungava
32 transform fault system developed due to the lateral offset between the Labrador Sea
33 and Baffin Bay. This lateral offset was established in the first rift stage possibly due
34 to the presence of the Nagssugtoqidian and Torngat terranes being less susceptible to
35 rift propagation. Without the influence of pre-existing structures the manifestation of
36 deformation cannot be easily explained during either of the rifting phases. Although
37 basement control diminished into the post-rift, the syn-rift basins from both rift stages
38 continued to influence the location of sedimentation possibly due to differential
39 compaction effects. Variable lithospheric strength through the rifting cycle may
40 provide an explanation for the observed diminishing role of basement structures
41 through time.

42 **Introduction**

43 Understanding the mechanisms that govern continental breakup is crucial to further
44 our understanding of the behaviour of the crust under extension (e.g. McKenzie,
45 1978; Lister *et al.*, 1991). Furthermore, such understanding is crucial in reducing the
46 exploration risk at rifted continental margins by providing constraints for models and
47 concepts used in exploration (e.g. Skogseid, 2001). One such group of interrelated
48 mechanisms that may control various aspects of continental breakup is the influence
49 of pre-existing geological structures (e.g. Theunissen *et al.*, 1996; Thomas *et al.*,
50 2006; Corti *et al.*, 2007; Gibson *et al.*, 2013; Manatschal *et al.*, 2015; Chenin *et al.*,
51 2015; Autin *et al.*, 2013; Petersen & Schiffer, 2016; Phillips *et al.*, 2016; Schiffer
52 *et al.*, in press). Here, we investigate the role that pre-existing structures potentially
53 played in continental breakup between Greenland and North America.

54 Pre-existing structures are defined as mechanical anisotropies in the pre-rift rocks that
55 occur on a variety of scales from metamorphic mineral fabrics to major tectonic
56 boundaries (Chattopadhyay & Chakra, 2013). Tectonic inheritance is the process by
57 which pre-existing structure may influence a subsequent geological event (e.g.

58 Holdsworth *et al.*, 2001; Huerta & Harry, 2012). A complete geological cycle of
59 tectonic inheritance has been proposed in which continental breakup occurs along the
60 major weaknesses formed by older orogenic belts (Wilson, 1966; Ryan & Dewey,
61 1997; Petersen & Schiffer, 2016; Schiffer *et al.*, in press), although in certain
62 instances orogenic activity may actually produce stronger lithosphere that is in fact
63 harder to rift (Krabbendam, 2001). Previous work has shown that pre-existing
64 structures can profoundly influence numerous aspects of the rifting process including;
65 magmatism (Bureau *et al.*, 2013; Koopmann *et al.*, 2014), sedimentary basin
66 geometry (Morley *et al.*, 2004), fault locations and timing (Korme *et al.*, 2004).

67 The rejuvenation of pre-existing crustal and lithospheric features during later tectonic
68 events occurs via two related processes; reactivation and reworking (Dore *et al.*,
69 1997; Holdsworth *et al.*, 1997, 2001; Houseman & Molnar, 2001). Reactivation
70 involves the rejuvenation of discrete structures (Butler *et al.*, 1997; Bellahsen *et al.*,
71 2006; Wu *et al.*, 2016), whereas reworking involves repeated focusing of
72 metamorphism, deformation or magmatism on the same crustal or lithospheric
73 volume (e.g. craton reactivation – Tappe *et al.*, 2007; repeated metamorphism –
74 Manhica *et al.*, 2001; large-scale barriers to rift propagation – Koopmann *et al.*,
75 2014). However, both reactivation and reworking may represent the same processes
76 operating at different scales and thus some ambiguity exists in distinguishing between
77 these two processes in the literature (Holdsworth *et al.*, 2001). Of particular relevance
78 to this study is the reactivation of discrete structures as a possible mechanism to
79 produce normal faults that are not perpendicular to regional extension (e.g. Morley
80 *et al.*, 2004; De Paola *et al.*, 2005) and the role of large-scale basement terranes
81 during rifting (e.g. Krabbendam, 2001). In this study we consider the roles of both
82 reactivation and reworking as end-member processes, both of which could have
83 influenced the incomplete breakup of Greenland and North America in the Davis
84 Strait.

85 **Rifting between Greenland and Canada**

86 The Labrador Sea and Baffin Bay (Fig. 1) formed due to divergent motion between
87 Greenland and North America (e.g. Chalmers & Pulvertaft, 2001). According to
88 Oakey & Chalmers (2012), breakup in this region occurred in three stages: (i) the
89 Palaeocene separation between North America and Greenland which was still

90 attached to Eurasia, (ii) the Eocene continued separation between Greenland and
91 North America at the same time as separation between Eurasia and Greenland
92 (Greenland moving as a separate plate) and (iii) since the Oligocene continued
93 separation between Eurasia and Greenland with the latter attached to North America,
94 i.e. the cessation of seafloor spreading to the west of Greenland (Fig. 2a).

95 Continental breakup between West Greenland and Eastern Canada resulted in oceanic
96 spreading in the Labrador Sea and Baffin Bay but not the Davis Strait (Fig. 2a). The
97 earliest rifting and the oldest, most extensive oceanic crust in the Labrador Sea –
98 Baffin Bay system is found in the Southern Labrador Sea (e.g. Srivastava, 1978).
99 Although lithospheric stretching in Baffin Bay is considered to have been sufficient to
100 initiate seafloor spreading (Suckro *et al.*, 2012) the extent of oceanic crust in Baffin
101 Bay is less than that of the Labrador Sea (e.g. Srivastava, 1978). The Davis Strait is a
102 bathymetric high, primarily consisting of continental crust (Dalhoff *et al.*, 2006),
103 linking the small oceanic basins of the Labrador Sea and Baffin Bay via the Ungava
104 Fault Zone (UFZ) (Suckro *et al.*, 2013). The UFZ may represent a ‘leaky transform’
105 (Funk *et al.*, 2012) with small amounts of oceanic crust produced at pull-apart basin
106 type settings but not full oceanic spreading (Srivastava, 1978).

107 The abundance and type of igneous rocks (Fig. 2a) also varies along the West
108 Greenland Margin (e.g. Keen *et al.*, 2012). The margins of the southern Labrador Sea
109 are non-volcanic (Chian *et al.*, 1995), however, they are volcanic in the northern
110 Labrador Sea, Davis Strait (Keen *et al.*, 2012) and Baffin Bay (Suckro *et al.*, 2012).
111 The Davis Strait is classified as a volcanic passive margin (Chalmers, 1997) due to
112 the presence of volumetrically extensive igneous rocks (Storey *et al.*, 1998) and a 4-
113 to 8-km-thick high velocity underplated layer (Funk *et al.*, 2007).

114 **Basement terranes of west Greenland and north-eastern Canada**

115 To determine the relationship, if any, between pre-existing geological structures and
116 margin forming processes it is crucial to understand: (i) the sequence of events prior
117 to rifting; (ii) the nature of the structural heterogeneities produced by previous events
118 and (iii) the orientation of subsequent rifting with respect to pre-existing structures.

119 *Nagssugtoqidian and Torngat Orogens*

120 The Nagssugtoqidian Orogen (NO) is a belt of Paleoproterozoic deformation and
121 metamorphism in West Greenland considered to have developed simultaneously with
122 the Torngat Orogen (TO) in Labrador (Fig. 2b). The TO and NO belts are interpreted
123 to have formed part of the same Paleoproterozoic passive margin prior to ocean
124 closure and continental collision (Van Gool *et al.*, 2002; Grocott & McCaffrey, 2017).
125 A continental collision model of formation is preferred over earlier interpretations of
126 an intracontinental strike-slip setting due to the presence of Paleoproterozoic calc-
127 alkaline dykes that are attributed to a subduction zone-type setting (Korstgård *et al.*,
128 1987). Reworked Achaean gneisses form a large majority of the NO (Van Gool *et al.*,
129 2002). The NO contains multiple onshore structures that represent candidates for
130 reactivation and reworking during rifting (Wilson *et al.*, 2006).

131 *The North Atlantic Craton and Nain Province*

132 The North Atlantic Craton (NAC) is the Achaean terrane immediately to the south of
133 the NO and north of the Ketilidian Mobile Belt (KMB) (Nutman & Collerson, 1991)
134 (Fig. 2b, spanning the interval 3850–2550 Ma (Polat *et al.*, 2014). The Nain Province
135 (NP) of Labrador is considered to be the North American continuation of the NAC
136 (St-Onge *et al.*, 2009) (Fig. 2b). As with the NO, the NAC also contains multiple
137 onshore structures that represent candidates for rejuvenation during rifting (Japsen
138 *et al.*, 2006).

139 **Methodology and datasets**

140 Two 2D seismic surveys were used in this study; the Spectrum West Greenland 2012
141 Repro and the BGR-77 survey alongside data from six exploration wells (Table 1 and
142 Fig. 1). Interpretation and analysis of the data primarily utilized Schlumberger's
143 Petrel, with further analysis conducted in ArcGIS, MATLAB and Generic Mapping
144 Tools (GMT version 5). Seismic line spacing is variable from approximately 5–20 km
145 in the south to 30–40 km in the north of the study area.

146 Table 1. Summary of exploration wells used in this study in the Davis Strait with the
147 terminal depth (TD) in metres from the rotary table. Lithology at TD from Nøhr-
148 Hansen (2003) and Rolle (1985)

149 *Seismic interpretation*

150 Twelve key seismic horizons, typically unconformities or high amplitude reflectors
151 (Fig. 3), were traced across the data (Figs 4 and 5). The six exploration wells were
152 then tied to the seismic data using the checkshots, with the seismic-well ties checked
153 against the same ties reported in previous studies (Dalhoff *et al.*, 2003; Døssing,
154 2011). The seismic horizons were then dated using the nearest biostratigraphically
155 dated samples in the wells (Rolle, 1985; Nøhr-Hansen, 2003; Piasecki, 2003;
156 Rasmussen *et al.*, 2003). Where no material in the well was identified for a desired
157 interval the position in the well was estimated by tracking seismic horizons that have
158 been tied to surrounding wells and using the next oldest and youngest defined
159 intervals as guidance. Some horizons were traced across the study area that could not
160 be exactly tied to dated horizons in any well. This applied to six horizons in this
161 study, two of which occur between the Late Lutetian and Middle Ypresian (the
162 Middle Eocene 1–2 horizons), whereas the other three are between the basement
163 horizon and the Late Thanetian (the Pre-Late Thanetian horizons 1–4). The horizons
164 were then used to generate seismic surfaces, and then in turn used to generate
165 isochrons. Isochrons were produced for the total sediment thickness (TST – seafloor
166 to basement) and for intervals between 11 interpreted horizons between the seafloor
167 and the basement within the polygon (Fig. 1).

168 *Fault mapping and analysis*

169 Faults that offset the top basement horizon were interpreted on individual seismic
170 lines. These faults were then, where possible, linked between seismic lines based on
171 orientation, size, style and proximity to one another and the free air gravity anomaly
172 (FAA – Sandwell *et al.*, 2014) was used to guide fault interpretation. In total, 66 faults
173 that offset the basement horizon were significant enough to tie between at least two
174 seismic lines.

175 Polyline shapefiles depicting the faults were then created in ArcGIS, allowing an
176 orientation analysis to be performed. Analysis of the fault population orientations was
177 calculated for (i) the complete fault and (ii) for fault segments generated by splitting
178 the polyline at the vertices prior to azimuth calculation. The second method provided
179 a more realistic representation of fault orientation as many of the faults change

180 azimuth along strike. Furthermore, a length scaling method was applied in order to
181 incorporate the influence of structure size into our analysis of fault sets. The length
182 scaling method used counts a particular fault (or fault segment) azimuth towards the
183 corresponding azimuth bin total the same number of times as the fault length in km.
184 For example in this analysis a structure of 1 km in length would be counted once,
185 whereas a structure 100 km in length would be counted 100 times. This results in a
186 scaled fault index rather than an absolute number of faults. Therefore, in order to fully
187 characterize the distribution of faults into structural sets it was necessary to consider
188 both the original (whole and split faults) in addition to the length scaled analysis.

189 *Study limitations*

190 Problems associated with the spatial distribution of the data are somewhat overcome
191 by integration of the discrete seismic and well data with the continuous free air
192 gravity and bathymetric data, whereas the effects of seismic line distribution was
193 shown to be minimal by the grid thinning (Fig. 6). Another potential issue was
194 utilizing biostratigraphic ages from the exploration wells (Nøhr-Hansen, 2003) as
195 none of the wells penetrate deep into the syn-rift (Table 1). Also tracking seismic
196 horizons over basement highs was problematic in small proximal basins without
197 wells. During the fault mapping the method of only analysing faults capable of being
198 tied between seismic lines could have induced spatial aliasing into our analysis. This
199 is particularly relevant if the large faults follow a different trend to faults smaller than
200 the seismic resolution. Finally, linking faults between 2D seismic lines may have
201 resulting in miss-tied faults given that it cannot be indisputably determined using this
202 type of data if faults are linked and if so what the nature of the link is, i.e. whether
203 they are hard or soft-linked.

204 **Results**

205 Seismic horizons

206 *Basement horizon*

207 The rift-onset unconformity representing the basement horizon is a high amplitude
208 reflector, between reflectors that display minimal organization and overlying
209 reflections that are mostly characterized by conformable packages of sediments, some

210 of which contain relatively high amplitude reflectors (Figs 4 and 5). Although little
211 organization is displayed in the reflectors beneath this horizon (Fig. 5, line E), some
212 high amplitude reflectors are present beneath which may represent intrusive rocks.

213 *Pre-Late Thanetian Marker 4 (PLT 4)*

214 This horizon is mostly represented by a high amplitude reflector or reflectors. PLT 4
215 is an unconformity, probably equivalent to the Middle Cretaceous Unconformity in
216 Sørensen (2006). The reflectors that comprise PLT 4 are usually discontinuous but the
217 horizon as a whole is easily recognized as the first high amplitude reflector above the
218 basement horizon. The reflectors below are sometimes chaotic with individual
219 horizons sometimes being difficult to distinguish and trace laterally, where they can
220 be distinguished they are often truncated by PLT 4. The packages of sedimentary
221 rocks beneath PLT 4 expand towards the footwalls of the faults that cut through PLT
222 4.

223 *Pre-Late Thanetian Marker 3 (PLT 3)*

224 PLT 3 lies conformably within the seismic sequence and is characterized by higher
225 amplitude than the surrounding reflectors. The sequences between PLT 3 and 4 can
226 been seen in some areas to expand away from basin bounding faults into the hanging
227 wall sediments and in many locations to be crosscut by discontinuous, concave
228 upwards, high amplitude reflectors most likely representing igneous intrusions (Fig. 4,
229 line A), with a doming of the horizons above (forced folds – Magee *et al.*, 2016). This
230 horizon downlaps onto the PLT 4 and basement horizons (Fig. 4, line A; & Fig. 5,
231 line E).

232 *Pre-Late Thanetian Marker 2 (PLT 2)*

233 The PLT 2 horizon lies conformably within the seismic sequence. The reflectivity of
234 the surrounding sequences is variable from transparent to high amplitudes but PLT 2
235 always represents a higher amplitude horizon than the surrounding sequences.

236 *Pre-Late Thanetian Marker 1 (PLT 1)*

237 The PLT 1 marker is a conformable, slightly higher amplitude horizon within a
238 relatively seismically transparent sequence. The package of reflections between PLT

239 2 and 1 thins from the centre of the study area to the north and south. On some
240 profiles this horizon can be difficult to distinguish from the seismically transparent
241 sequences in nearby proximity.

242 *Late Thanetian (~54 Ma)*

243 The Late Thanetian horizon is one of the key horizons interpreted as it is easily
244 recognizable across the area and it represents an unconformity in the south of the area
245 which potentially extends to the north. Sørensen (2006) recognized a Late Cretaceous
246 unconformity which we interpret as erosion of sequences prior to this horizon. This
247 horizon manifests in many areas as a high amplitude reflector, possibly from the
248 Palaeogene flood basalts (e.g. Larsen *et al.*, 1999). The packages from the four PLT
249 horizons are truncated by the Late Thanetian horizon.

250 *Middle Ypresian (~53 Ma)*

251 This high amplitude horizon lies immediately above the unconformity at the top of a
252 seismically low amplitude package of conformable sequences. The reflectors
253 comprising this horizon are generally continuous (Fig. 4, lines B & C; Fig. 5, line D)
254 except when this horizon is close in TWTT to the Late Thanetian horizon (Fig. 4, line
255 A).

256 *Middle Eocene Marker 2 (ME 2)*

257 The ME 2 horizon is equivalent to the Middle Eocene unconformity (Sørensen, 2006).
258 The nature of the reflectors constituting the ME 2 horizon varies across the study area,
259 although its characteristics are sufficiently consistent for interpretation. ME 2 is
260 located between a chaotic sediment package in which individual horizons are difficult
261 to determine and the continuous sub-parallel overlying horizons. Where the
262 surrounding packages are thinner in TWTT ME 2 is difficult to interpret, particularly
263 in the south.

264 *Middle Eocene Marker 1 (ME 1)*

265 ME 1 is a conformable, slightly higher amplitude horizon, within a low amplitude
266 package. The reflectors that comprise this horizon (Fig. 4, line B & Fig. 5, line D) are

267 usually discontinuous and stratigraphic relationships are sometimes difficult to
268 interpret.

269 *Late Lutetian (~41 Ma)*

270 The late Lutetian horizon is a high amplitude reflector at the top of a low amplitude
271 package, comprising sub-parallel reflectors, although in some areas it is chaotic and
272 indistinct. The package of horizons between the Late Lutetian and the ME 1 expands
273 northwards, containing many horizons that could be traced locally, and may belong to
274 the Kangâmiut formation which is present in the north but not the south (Sørensen,
275 2006) (Fig. 3).

276 *Base Early Pliocene (~5 Ma)*

277 This horizon is equivalent to the Late Miocene unconformity (Sørensen, 2006)
278 (Fig. 3), and is mostly characterized by medium to high amplitude reflectors. The
279 sequences above downlap onto this horizon (Fig. 4, line D) and the stratigraphic
280 successions above are typically sub-parallel, although sigmoidal packages are also
281 present. The sequences above and below this horizon are discontinuous, particularly
282 above basement highs in the south.

283 *Late Pliocene (~3 Ma)*

284 The Late Pliocene horizon is represented by conformable medium amplitude
285 reflectors (Figs 4 and 5), which are mostly sub-parallel, although in the central and
286 southern parts of the study area the packages beneath the Late Pliocene horizon are
287 sigmoidal and discontinuous. Small disturbances to this horizon coincide with
288 bathymetric lows, possibly representing disruption by fluid movements.

289 *Seismic surfaces*

290 The basement topography (Fig. 7A) is a high relief surface with lows below 7000 ms
291 TWTT, whereas in other areas basement highs can be seen to be near the seafloor. In
292 contrast the present bathymetric surface (Fig. 7M) is a low relief with essentially three
293 key features: (i) a shallow water platform in the north and east; (ii) a deeper area
294 occupying the area southwest and (iii) a channel incised to 3000 ms TWTT on the
295 southern edge of the polygon.

296 Similarities exist between the basement (Fig. 7A) and the current bathymetric
297 surfaces (Fig. 7M) including: (i) the elongate margin parallel basement high along the
298 eastern edge of the polygon approximates the broad bathymetric high; (ii) some
299 basement highs in the south are expressed as bathymetric highs and (iii) the elongate
300 north-south basement low in the south coincides with the incised channel on the
301 modern bathymetry. However, as expected the modern bathymetry more closely
302 resembles the horizons interpreted within the post-rift (e.g. Fig. 7F–M), with the
303 degree of similarity increasing as the post-rift progresses. Overall, through time the
304 relief (horizon topography in TWTT) on the interpreted surfaces can be seen to
305 progressively decrease.

306 Seismic isochrons

307 The isochrons are shown in Figs 8 and 9. In this section the terms ‘sedimentation’ and
308 ‘deposition’ are used to refer to the time thickness infill recorded on the isochrons in
309 TWTT (ms) that may also include volcanic rocks and does not make inferences about
310 the rate of infill or amount of sediment flux.

311 *Total sediment thickness*

312 Total Sediment thickness (TST; Fig. 8a) was calculated between the seafloor and the
313 basement horizon. Deep basins (>5000 ms TWTT) occur in the southern, central and
314 northern parts of the study area. These deep basins form an approximately margin
315 parallel chain with the major depocentres connected by thinner area of c. 3000 ms
316 TWTT. Basins do occur outside of this chain across much of the south and in some
317 isolated areas of the north but do not exceed c. 3000 ms TWTT and are spatially
318 smaller (Fig. 8b).

319 Comparison of the TST isochron and the Bouger gravity anomaly (Fig. 8a & d) shows
320 that the distribution of sedimentary basins alone does not explain the Bouger gravity
321 anomaly. If the sedimentary basins are the sole contribution to the gravity anomalies
322 it would be expected that gravity lows should coincide with deep basins and gravity
323 highs with basement highs. Thus, because this relationship is not observed deeper
324 structures must account for the variation in the anomalies. In the north of the area
325 deep basins do coincide with gravity highs. However, it can be seen that the deep

326 NNE-SSW trending basin in the south has only a slightly lower gravity anomaly of c.
327 15–40 mGal compared with that of its surroundings of c. 40–80 mGal.

328 *Large-scale temporal evolution: Basement to Late Thanetian and Late Thanetian to*
329 *seafloor*

330 Isochrons have not been produced for intervals that can be explicitly defined as syn-
331 rift and post-rift, as it is unlikely that rifting ceased simultaneously across the study
332 area, particularly given that multiple rifting events occurred (e.g. McGregor *et al.*,
333 2012). Instead, the Late Thanetian has been chosen to approximate the syn- to post-
334 rift transition as it represents the first dated horizon and significantly different infill
335 styles operate before and after (Fig. 9). Thus, comparison of pre- and post-Late
336 Thanetian infill provides insights into the long-term differences between the early and
337 late evolution of the study area.

338 The time thickness between the basement horizon and the Late Thanetian often
339 represents the period of thickest sedimentary infill with over c. 3000 ms TWTT in
340 many basins, particularly in the south (Fig. 8b). The largest depocentre is the NNE-
341 SSW chain of basins in the south, but other significant depocentres are present.
342 During this interval a distinct north-south disparity in basin aspect ratio is apparent,
343 with the basins in the south tending to be more elongate than basins in the north.

344 The interval between the Late Thanetian and the modern seafloor (Fig. 8c) is
345 dominated by a singular, elongate, margin parallel basin that for large parts is c.
346 4000 ms TWTT thick. Outside of the dominant basin preserved time thickness rarely
347 exceeds c. 1500 ms TWTT.

348 Comparison between the pre- and post-Late Thanetian isochrons (Fig. 8b and c)
349 shows that the large basins in the south received a greater amount of their time
350 thickness infill during the earlier interval, whereas the large basin in the north
351 received more during the later interval. Significant basins are located in the north of
352 the study area during the latter interval but no significant time thickness infill is
353 recorded in the south during the latter interval.

354 In summary, during the earlier interval deposition dominates the south in small
355 discrete basins, whereas the later interval is dominated by more diffuse infill in the

356 north. However, despite the large-scale difference observed between infill in the pre-
357 and post-Late Thanetian intervals many areas that record lower time thickness infill
358 during the earlier interval continue to receive lower amounts during the later interval.
359 In addition, areas occupied by major basins during the earlier interval continue to
360 record slightly higher infill than their surroundings in the later interval. The notable
361 exception to this is in the southeast, where significant infill characterizes the earlier
362 interval, whereas minimal infill is record in the later interval.

363 *Onset of rifting to Late Thanetian*

364 This is the interval between the basement and our first dated horizon (Late Thanetian)
365 (Fig. 9A–E). Having considered the interval as a whole in the last section, here we
366 focus on the detail shown by markers PLT 1-4 from oldest to youngest.

367 Between the basement horizon and the PLT marker 4 (Fig. 9A) many small
368 depocentres are present across the study area. Some deposition occurred along the
369 location of the major elongate basin(s) in the south of the study area where
370 subsequent intervals also show significant infill.

371 Between the PLT marker 4 and PLT marker 3 (Fig. 9B) this major north-south basin
372 in the south of the study area dominates deposition and the small depocentres which
373 characterized the previous interval are less abundant. Some of the large depocentres
374 from the previous interval, particularly in the central and northern parts of the study
375 area, are now characterized by areas of lower sedimentation.

376 Between PLT Markers 2 and 3 (Fig. 9C), infill is characterized by diffuse deposition
377 particularly in the northeast and southwest of the study area and deposition in the
378 north-south elongate basin is lower than the previous two intervals.

379 The interval between PLT Markers 2 and 1 (Fig. 9D) records low sedimentation in a
380 broadly similar distribution to the last interval. The largest depocentre in this interval
381 is the area of diffuse sedimentation in the north where up to c. 500 ms TWTT of
382 sediments are present.

383 Between PLT Marker 1 and the Late Thanetian horizon (Fig. 9E) the northern area is
384 now one of minimal sedimentation, whereas infill accumulated in the small basins in

385 the south with slightly thicker infill recorded at the location of the major southern
386 basin that was identified during previous intervals.

387 *Late Thanetian to Middle Ypresian*

388 This interval (Fig. 9F) shows a different distribution of depocentres compared to
389 previous intervals that resulted in distinct differences between infill patterns in the
390 north and south. The area of thickest infill is a poorly defined basin in the north with
391 lobes trending to the east and south away from the maximum thickness to the
392 northwest. This depocentre appears to extend beyond our polygon with the greater
393 infill to the west. The southern part of the study area during this interval is
394 characterized by lower time thickness infill not exceeding c. 1000 ms and mostly less
395 than c. 250 ms. Despite the southern area recording lower infill overall compared to
396 the north, relatively more infill is recorded at the location of the major southern basin
397 identified during previous intervals.

398 *Middle Ypresian to Late Lutetian*

399 The dominant basin between the Middle Ypresian and Mid Eocene Marker 2
400 (Fig. 9G) is coast parallel, displaying diffuse infill of c. 400 ms TWTT, with a step to
401 the east in the south with the area of maximum infill located at the northern end of
402 this basin. Between Mid Eocene marker 2 and Mid Eocene marker 1 (Fig. 9H) this
403 basin shows a considerably reduced aspect ratio, with maximum thickness now
404 located in the centre. A significant depocentre subsequently develops in the central
405 northern part of the study area from Mid Eocene marker 1 to the Late Lutetian
406 (Fig. 9I) containing c. 800 ms (TWTT) of infill. Outside of this major basin minimal
407 sedimentation is recorded, particularly in the south.

408 *Late Lutetian to early Pliocene*

409 During this interval (Fig. 9J) significant depocentres were present in the north,
410 whereas the central and southern areas record thin diffuse infill. Two small
411 depocentres on the southern margin of the polygon are present, with the eastern most
412 of these coinciding with the major elongate basin that dominated the southern part of
413 the study area during the pre-Thanetian time intervals.

414 *Early Pliocene to late Pliocene*

415 During this interval (Fig. 9K) maximum sedimentation occurred in a basin in the
416 centre of the polygon, where c. 400–800 ms (TWTT) is present. The significant
417 basins in the north during the last interval are no longer present, with the north now
418 recording reduced amounts of infill.

419 *Late Pliocene to present*

420 This interval (Fig. 9L) represents a period of significant deposition; particularly in the
421 central and eastern areas. During this interval up to c. 1200 ms TWTT of infill was
422 deposited in the centre of the main coast parallel basin.

423 *North-south disparity*

424 A north-south division is present on many of the isochrons and in the Bouguer gravity
425 anomaly (Fig. 8d). Such a division is apparent on the Late Thanetian and the Middle
426 Ypresian isochron (Fig. 9F) and on the Middle Eocene Marker 1 to the Late Lutetian
427 isochron (Fig. 9I). In both of these intervals much greater amount of time thickness
428 infill is recorded in the north than in the south. A north-south disparity is also
429 observable in the earliest isochrons where southern basins have a much greater aspect
430 ratio than northern basins. Bouguer gravity data also show north-south disparity with
431 a strong positive anomaly across the south and a strong negative anomaly across
432 much of the north (Fig. 8d).

433 *Fault interpretation and mapping*

434 This section describes the faults interpreted on seismic reflection profiles and the fault
435 map.

436 *Fault interpretation*

437 All of the interpreted horizons are offset by normal faults, although fault offsets are
438 larger (often >1000 ms) and faulting is more widespread within the lower (pre- PLT
439 2) successions. Normal fault offset is highly variable, although no particular area is
440 dominated by much larger fault throws than elsewhere. Basement horizon offset of c.
441 1000 ms by normal faults is common with offsets up to c. 4000 ms being observed on

442 the westward dipping normal fault bounding the large elongate N-S basin in the south.
443 Dip generally decreases with depth on the large normal faults (offset >1000 ms) that
444 offset the basement horizon.

445 Reverse faulting was also observed in proximity to the Ikermiut Fault Zone (IFZ –
446 Gregersen & Skaarup, 2007; Chalmers & Pulvertaft, 2001). In the IFZ reverse
447 faulting in close association with folding affects the successions prior to the Middle
448 Ypresian Horizon (Fig. 5, Line D and Fig. 10, Line F). Thus, the age of this
449 deformation is post-Middle Ypresian and pre-Middle Eocene 2. Folding was also
450 observed in absence of reverse faulting but it more commonly occurs alongside
451 reverse faults. Although several reverse faults were interpreted it was only possible to
452 tie one of these across multiple (three) seismic lines (reverse fault 2 – Fig. 10).

453 *Fault mapping*

454 Fault mapping was conducted within the primary study area defined by the polygon
455 (Fig. 1a) and further south along the West Greenland margin (Fig. 11). The extension
456 to the south in which fault mapping was conducted was not included in the seismic
457 horizon analysis due to the lack of well coverage, prohibiting a comparably reliable
458 analysis from being conducted. Most faults have been mapped at depths of between
459 3000 and 6000 ms TWTT, however, a number of the larger faults reach depths of
460 7000 ms TWTT. The centre of the study area contains the highest density of shallow
461 basement offsetting faults, which in some cases do not exceed depths of 4000 ms
462 TWTT. The azimuth of the fault planes varies along strike on most of the faults and
463 some also display variation in azimuth down dip on the fault plane. Thus, when
464 analysing orientation the faults were divided into segments. Overall, it can be seen
465 that the southern and central areas may contain a considerably greater density of
466 normal faults. However, this could be due to sampling bias as a result of the denser
467 seismic grid in the south.

468 The geographical distribution of faults mapped in our work is similar to the previous
469 interpretation shown in Chalmers & Pulvertaft (2001) based on Chalmers, (1991) and
470 Chalmers & Laursen, (1995), with the largest faults in our study corresponding with
471 the majority of faults shown in Chalmers & Pulvertaft (2001). The principal
472 difference between these interpretations is apparent in the south where the faults have

473 now been mapped in greater detail due to the availability of more recent data. Several
474 areas where no faults are shown on the Chalmers & Pulvertaft (2001) map have now
475 been shown to have observable faults.

476 Analysis of fault strike is shown on rose diagrams in Fig. 12, with each fault analysed
477 as a single polyline (Fig. 12a, b, e & f) and divided up at its vertices (Fig. 12c, d, f, g
478 & h). In the non-length scaled results $n=66$ when the faults are not split at their
479 vertices and $n=152$ when the faults are split at their vertices. The results of length
480 scaling the fault population are shown on Fig. 12e–h. Based on orientation three fault
481 sets were recognized in addition to the Ikermit reverse faults. These are as follows:
482 NE-SW (Fault Set 1), NNW-SSE (Fault Set 2) and NW-SE (Fault Set 3). The NNW-
483 SSE oriented Fault Set 2 is more prominent when analysing the faults as segments
484 divided on their vertices and when scaled by length. The longest faults and the faults
485 with the largest (>3000 ms TWTT) offsets belong to fault sets 2 and 3. However,
486 large faults do exist in fault set 1. The longest fault (c. 220 km long) belongs to fault
487 set 3. The largest fault in fault set 1 occurs in the southeast of the interpretation
488 polygon and is c. 60 km long, whereas the longest fault in fault set 2 is c. 120 km
489 long.

490 Most of the brittle deformation documented in this study occurs prior to the Late
491 Thanetian Horizon and in particular prior to the PLT 4 horizon (e.g. Fig. 4, lines a &
492 c). However, it is evident that some deformation continues on rift-related structures
493 into the Eocene successions, potentially due to differential sediment compaction
494 between the syn-rift basins and highs. However, within the resolution of the data it
495 was not possible to either relatively or absolutely constrain the timing of movement
496 on each of the normal fault sets using the individual seismic lines, the surfaces or
497 isochrons. This is evident on the earliest isochron from the Basement to the PLT 4
498 horizon whereby basins with orientations corresponding to all the fault sets identified
499 can be seen to have formed (Fig. 9A). The reverse faults documented in the IFZ
500 (Fig. 10) do not appear to extend beyond the Middle Ypresian.

501 **Discussion**

502 Through time the location and nature of the thickest infill in the area has changed
503 from occurring in discrete fault bound basins, to more diffuse broad regions of infill

504 (Fig. 9). Here, the cause of this changing distribution is considered, alongside the
505 relationship of the offshore structures and those previously published from onshore
506 (Japsen *et al.*, 2006; Wilson *et al.*, 2006).

507 *Comparison of on and offshore structures*

508 The study area lies adjacent to both the NO and the NAC (Fig. 2b) but as the offshore
509 continuation of the boundary between these terranes cannot be precisely located
510 structures in both terranes are considered as candidates for rejuvenation. The north-
511 south division displayed in many of the results of this study (e.g. fault density and
512 basin size; Fig. 9F and I) may be linked to the location of the boundary between the
513 Achaean NAC and the Proterozoic NO. Alternatively, the north-south division may be
514 an artefact of the uneven distribution of the data, although the quality control grid
515 thinning (described in the methodology) suggests that the influence of line density is
516 minimal (Fig. 6), which indicates a geological explanation for this observation is
517 plausible.

518 In addition to the boundary between the NO and the NAC (Fig. 2b) significant
519 structural divisions within the NO may have also undergone rift-related reactivation,
520 influencing the development of the offshore region. For example, comparison of the
521 onshore geological map and cross section of Van Gool *et al.* (2002) (Section G) with
522 an adjacent seismic line (Line G) from the offshore region (Fig. 13) demonstrates that
523 the offshore continuation of the Nordre Strømfjord shear zone (NSSZ), Nordre
524 Isortoq shear zone (NISZ) and Ikertôq thrust zone (ITZ) may correspond to distinct
525 structures observable on this seismic line. In particular, on Line G it appears that the
526 ITZ may correspond to the bounding fault of the basin shown on this line as the
527 approximate continuation of the ITZ would be expected here, the dip direction of the
528 basin bounding fault is similar and the reflection characteristics of the basement either
529 side of this structure are what would be expected based on the onshore geology, i.e.
530 the folded fabrics of the CNO and SNO display different internal reflectivity
531 compared to within the ITZ (Wilson *et al.*, 2006).

532 All three major fault sets identified in this work (Figs 11 and 12) correspond to
533 structural systems identified onshore by Wilson *et al.* (2006) in the NO (Table 2).
534 Purely based on orientation, without implying a causative link, the orientation of fault

535 set 1 (NE-SW) in this study is similar to systems 1 (ENE-WSW) and 4 (NNE-SSW),
536 fault set 2 (NNW-SSE) in this study is the same orientation as system 3 (NNW-SSE),
537 whereas fault set 3 (NW-SE) in this study is of a similar orientation to systems 3
538 (NNW-SSE) and 5 (E-W to ESE-WNW) in Wilson *et al.* (2006). Given the close
539 orientation of fault sets 2 and 3 in this study it cannot be determined to which of these
540 fault sets system 3 in Wilson *et al.* (2006) may correspond to. Thus, system 3 in
541 Wilson *et al.* (2006) is considered as a possible rejuvenation candidate for both fault
542 sets 2 and 3. Wilson *et al.* (2006) suggested that system 1 has a similar trend to the
543 dominant basement fabric in the NO, system 2 represents closely spaced faults often
544 showing both sinistral and normal offset, system 3 is a closely spaced set of faults
545 showing net dextral and normal offset of 20–40 m, system 4 structures are major
546 subvertical sinistral strike-slip faults and fault zones and system 5 is a relatively
547 localized set of dextral strike-slip structures.

548 The three major fault trends identified in this work also correspond to structural
549 systems observed onshore in the Achaean NAC (Japsen *et al.*, 2006). Correlation
550 based on orientation between the fault sets identified in this work and the outcrop
551 analysis of Japsen *et al.* (2006), again without implying a causative link shows that
552 fault set 1 (NE-SW) corresponds with the NE-SW trending deep gullies observed
553 onshore; fault set 2 (NNW-SSE) is of a similar orientation to the N-S trending
554 structure dipping moderately to the east, parallel to basement fabrics in the area; and
555 fault set 3 (NW-SE) is the same orientation as the NW-SE trending joints and
556 fractures which dip NE.

557 Comparison between on- and offshore structures demonstrates that there are certainly
558 similarly oriented structures present both on and offshore. However, determining
559 whether the structures are reactivated pre-existing structures or structures created
560 during Mesozoic rifting requires examination of fault orientations with respect to
561 rifting directions (e.g. Abdelmalak *et al.*, 2012). In the following sections fault
562 orientations and the distribution of basin infill are considered in the context of a two-
563 stage rifting model for the region (e.g. Wilson *et al.*, 2006; Abdelmalak *et al.*, 2012;
564 Oakey & Chalmers, 2012).

565 *Stage 1: rifting*

566 This rifting stage (Fig. 14b) encompasses the oceanic magnetic anomalies from at
567 least Chron 27 (ca. 62 Ma; Palaeocene), possibly earlier, to Chron 24 (ca. 54 Ma;
568 Eocene) (Abdelmalak *et al.*, 2012). However, extension in the region has been dated
569 as early as the Late Triassic, with intense lithospheric stretching in the Early
570 Cretaceous that produced dykes in West Greenland (Larsen *et al.*, 2009) and their
571 disputed minor equivalent in Labrador (Tappe *et al.*, 2007; Peace *et al.*, 2016). The
572 isochrons documenting sediment distribution during this early rift interval are those
573 prior to the Late Thanetian. Sediment deposition in this interval is focused into small
574 isolated, fault bound basins that are in many places organized into ~N-S oriented
575 chains (Fig. 9A and B).

576 The extension direction during this period was calculated by Abdelmalak *et al.* (2012)
577 to be $069^{\circ} \pm 10$ by inversion of fault-slip data using the inversion methodology
578 described in Angelier (1990). The stress inversion conducted in West Greenland
579 described by Abdelmalak *et al.* (2012) included 3300 measurements of fault-slip data
580 from 60 measurement sites located in Palaeocene to Eocene basaltic formations. Most
581 faults used in the Abdelmalak *et al.* (2012) inversion are relatively minor with throws
582 not exceeding a few decimetres.

583 Of the three offshore fault populations identified by this study (Fig. 12) the closest to
584 perpendicular to $069^{\circ} \pm 10$, as would be expected when rifting a homogenous
585 medium, is fault set 2 (NNW-SSE). Onshore in the NO domain Wilson *et al.* (2006)
586 showed that a set of NNW-SSE faults are not the youngest structures and typically
587 have a dextral strike-slip sense and that a N-S set of faults display normal and sinistral
588 senses of movement. Whereas in the NAC domain, Japsen *et al.* (2006) documented a
589 N-S structural trend as a prominent feature lying parallel to the basement fabric with a
590 dextral sense. The slightly off-perpendicular orientation of these onshore structures
591 with respect to rifting direction (Abdelmalak *et al.*, 2012) could be due to the
592 influence of a pre-existing structure set such as those identified onshore by Wilson
593 *et al.* (2006) or it could be due to the error associated with the stress inversion
594 (Abdelmalak *et al.*, 2012) or the fault orientation analysis in this study.

595 Fault set 3 is the most dominant offshore structural trend in terms of the absolute
596 number of faults and the size of the faults, some of which are the largest structures
597 identified. Given the abundance and size of fault set 3, this fault set appears to
598 represent the dominant manifestation of rift-related deformation. This is intriguing
599 given the orientation of fault set 3 with respect to the extension direction (Abdelmalak
600 *et al.*, 2012), which is difficult to reconcile without invoking the influence of pre-
601 existing structures. The onshore studies have found multiple candidate structural sets
602 that may have influenced the development of fault set 3. For example, onshore
603 structures oriented NW-SE were identified in the NAC domain by Japsen *et al.*
604 (2006). However, Japsen *et al.* (2006) were unable to determine any kinematic
605 indicators on their NW-SE system. Furthermore, in the NO Wilson *et al.* (2006)
606 identified a structural set oriented E-W to ESE-WSW which may also present a
607 candidate structural set that influenced the development of fault set 3.

608 The NE-SW oriented fault set 1 has comparable abundance to fault set 2 but it is near
609 parallel to the reconstructed extensional direction of $069^\circ \pm 10$ (Abdelmalak *et al.*,
610 2012). Thus, it is difficult to reconcile these structures being involved in early rifting
611 without invoking the reactivation of pre-existing structures in localizing deformation
612 and a significant oblique slip component. Candidates for pre-existing structures
613 related to fault set 1 are present onshore in the NAC domain where Japsen *et al.*
614 (2006) observed a NE-SW structural set characterized by easily distinguishable yet
615 poorly exposed deep, wide gullies. Furthermore, in the NO Wilson *et al.* (2006)
616 documented an ENE-WSW fault set parallel to basement structures, displaying
617 evidence for multiple phases and senses of movement. To summarize, fault set 1
618 would be unlikely to have developed without the influence of pre-existing structures.

619 Overall, during this interval fault location and orientation is primarily controlled by
620 pre-existing structures (Fig. 14b) with fault set 1 (NE-SW) representing a highly
621 oblique normal reactivation; fault set 2 (NNW-SSE) representing normal faults
622 approximately orthogonal to the rifting direction that possibly, but not necessarily,
623 always exploited pre-existing structures; and fault set 3 (NW-SE) representing
624 oblique normal reactivation.

625 Our kinematic model for rift development in this interval is in broad agreement with
626 the previously proposed reactivation model developed onshore that made predictions

627 for the offshore by Wilson *et al.* (2006). Given that faulting is strongly controlled by
628 pre-existing structures it follows that the location of depocentres during this interval,
629 as depicted on the isochrons prior to the Late Thanetian, was also strongly controlled
630 by pre-existing structures.

631 *Stage 2: rifting and transform development*

632 The second stage of extensional deformation (Fig. 14c) occurred between oceanic
633 magnetic anomalies Chron 24 (ca. 54 Ma; Eocene) to Chron 13 (ca. 35 Ma;
634 Oligocene), when Greenland moved north with respect to North America (e.g. Suckro
635 *et al.*, 2013), and regional extension has been calculated as ~N-S ($178^\circ \pm 10^\circ$ –
636 Abdelmalak *et al.*, 2012). The northward movement of Greenland caused sinistral
637 deformation (Wilson *et al.*, 2006) associated with the transform deformation on the
638 UFZ (Kerr, 1967) including the areas of transpression such as the IFZ (Fig. 10).
639 Deposition during this interval is minimal and chaotic in the south with poorly
640 defined basins, whereas in the north a new basin is present (Fig. 9F). This may reflect
641 deposition while a large-scale change in stress regime and rifting direction was taking
642 place.

643 No faults in the study area were documented perpendicular to the proposed ~N-S
644 extension direction (E-W) as would be expected under extension of a homogenous
645 medium. It is therefore possible that deformation during this interval was influenced
646 both by pre-rift structures and structures formed during stage 1 rifting. Although some
647 deformation likely continued on fault sets 1, 2 and 3 the primary manifestation of
648 deformation in this rifting stage is associated with the initiation and development of
649 the UFZ. Our proposed model for this transform fault system is that offset between
650 extension in Baffin Bay and the Labrador Sea was established during the first rifting
651 stage, possibly due to the rift being unable to fully propagate through the NO and TO
652 (Fig. 2b). Then in the second rifting stage when the extension vector changed to ~N-S
653 (Abdelmalak *et al.*, 2012) deformation was switched to transform system
654 development. Thus, unlike in the first rifting interval where the rejuvenation pre-
655 existing structures during rifting was through reactivation of discrete structures the
656 role of pre-existing structures during the second rift stage influenced the large-scale
657 manifestation of deformation through reworking as defined by (Holdsworth *et al.*,
658 2001).

659 The nature of reactivation and the role of pre-existing structures through time

660 Overall, we propose that pre-existing structures of various origins, that possibly
661 correspond to structures identified onshore (Japsen *et al.*, 2006; Wilson *et al.*, 2006),
662 directly facilitated the subsequent localization of deformation during rifting which
663 controlled the location and geometry of syn-rift deformation. We favour this over a
664 scenario whereby pre-existing structures facilitated the development of localized
665 stress fields which then interacted in the overburden to create structures oblique to the
666 extension direction. The reason for this is that the structures mapped (Fig. 11) were
667 observed to offset the pre-rift rocks (basement horizon) then not change strike
668 considerably through the overlying material as would be expected with interacting
669 stress fields.

670 Variable lithospheric strength through the rifting cycle may provide an explanation
671 for the diminishing role of basement structures through time. In particular during
672 stage 1 rifting where significant extensional deformation is inferred (Fig. 14b) it is
673 possible that this lithospheric thinning resulted in an elevated geothermal gradient
674 causing overall lithospheric weakening (Kusznir & Park, 1987). In such a situation
675 the lithosphere may approach an Airy isostasy type situation whereby isostatic
676 compensation would be extremely local, and may be accommodated by movement of
677 discrete pre-existing structures. As rifting diminished and eventually ceased, cooling
678 of the lithosphere would have resulted in an increase in lithospheric strength. Isostatic
679 compensation of a stronger lithosphere favours broad regional flexure rather than
680 localized faulting. Thus, the changing geothermal and strength profiles of the
681 lithosphere through the rift cycle may provide an explanation for the reduced role of
682 discrete, pre-existing structures through time, a possibility that should be investigated
683 by future work in both the Davis Strait and elsewhere.

684 During the post-rift interval some expressions of rifting can be identified despite the
685 influence of basement and rift-related structures diminishing. Firstly, the highs
686 produced during rifting are often situated in similar locations to bathymetric highs
687 (Fig. 7). The mechanism behind this phenomenon may be differential compaction,
688 whereby less compaction occurs in the areas of minimal cover (Mesozoic highs) due
689 to the presence of crystalline basement rocks. This mechanism may also explain why

690 areas that were basins in the syn-rift continue to receive greater amounts of infill
691 during the post-rift.

692 *Petroleum systems implications*

693 The small isolated basins depicted on the isochrons prior to PLT marker 3 (Fig. 9A–
694 D) would provide a suitable location for the accumulation of organic matter in a
695 spatially restricted environment that could lead to anoxic conditions indicative of
696 preservation of organic matter. However, these small basins could make potential
697 source rocks spatially limited and laterally variable. This is particularly important as
698 the source rock interval offshore West Greenland is within the Cretaceous successions
699 (Schenk, 2011). Finally, the thermal (e.g. Fjeldskaar *et al.*, 2008; Peace *et al.*, 2003)
700 and structural (e.g. Magee *et al.*, 2017) implications of the widespread magmatism
701 upon petroleum systems offshore West Greenland should also be considered during
702 exploration.

703 **Conclusions**

704 Three fault systems were identified in the Davis Strait: (i) NE-SW, (ii) NNW-SSE
705 and (iii) NW-SE, all of which correlate with structural trends identified onshore by
706 previous work. During the first phase of rifting, faulting was primarily controlled by
707 pre-existing structures with fault set 1 (NE-SW) representing oblique normal
708 reactivation; fault set 2 (NNW-SSE) representing normal faults approximately
709 orthogonal to extension possibly influenced by pre-existing structures and fault set 3
710 (NW-SE) representing oblique normal reactivation. In the second rifting stage, the
711 sinistral UFZ transform system developed due to the lateral offset between the
712 Labrador Sea and Baffin Bay. This lateral offset was established in the first rift stage
713 possibly due to the presence of the NO-TO belt being unsusceptible to rift
714 propagation. Without the influence of pre-existing structures the manifestation of
715 deformation cannot be easily understood in the context of previously published rifting
716 phases and directions.

717 The primary control on location and nature of rifting changed through time with
718 basement anisotropy providing the main control on early faulting. The role of faulting
719 and basement structures diminishes throughout the syn-rift and into the post-rift.
720 However, pre-existing structures influenced certain aspects of the post-rift. The

721 thermal regime and thus variations in lithospheric strength through the rift cycle may
722 provide an explanation for the diminishing influence of pre-existing structures
723 through time.

724 Finally, there is a distinct division between the north and south of the study area, with
725 the syn-rift being dominated by deposition in the south, and the post-rift being
726 dominated by deposition in the north. This long-lived division could reflect a
727 significant pre-existing structure, potentially the offshore continuation of the NAC
728 and NO boundary.

729 **Acknowledgements**

730 Funding for this research was primarily provided by Royal Dutch Shell in the form of
731 a CeREES studentship at Durham University. The Durham University Center for
732 Doctoral Training (CDT) in Energy and the Durham Energy Institute (DEI) are also
733 thanked for their contribution towards the costs of this research. We would also like to
734 thank Spectrum and BGR for providing access to the seismic data and Schlumberger
735 for the Petrel software. Finally, we thank Dr. Craig Magee and two anonymous
736 reviewers for their constructive reviews that significantly improved the quality of this
737 manuscript.

738 **Conflicts of interest**

739 No conflict of interest declared.

740 **References**

741 Abdelmalak, M.M., Geoffroy, L., Angelier, J., Bonin, B., Callot, J.P., Gélard, J.P. &
742 Aubourg, C. (2012) Stress fields acting during lithosphere breakup above a melting
743 mantle: a case example in West Greenland. *Tectonophysics*, 581, 132–143.

744

745 Angelier, J. (1990) Inversion of field data in fault tectonics to obtain the regional
746 stress-III. A new rapid direct inversion method by analytical means. *Geophys. J. Int.*,
747 103(2), 363–376.

748

749 Autin, J., Bellahsen, N., Leroy, S., Husson, L., Beslier, M.O. & D'Acromont, E.
750 (2013) The role of structural inheritance in oblique rifting: insights from analogue
751 models and application to the Gulf of Aden. *Tectonophysics*, 607, 51–64.

752

753 Bellahsen, N., Fournier, M., d'Acromont, E., Leroy, S. & Daniel, J.M. (2006) Fault
754 reactivation and rift localization: Northeastern Gulf of Aden margin. *Tectonics*, 25(1),
755 1–14.

756

757 Bureau, D., Mourgues, R., Cartwright, J., Foschi, M. & Abdelmalak, M.M. (2013)
758 Characterisation of interactions between a pre-existing polygonal fault system and
759 sandstone intrusions and the determination of paleo-stresses in the Faroe-Shetland
760 basin. *J. Struct. Geol.*, 46, 186–199.

761

762 Butler, R.W.H., Holdsworth, R.E. & Lloyd, G.E. (1997) The role of basement
763 reactivation in continental deformation. *J. Geol. Soc.*, 154(1), 69–71.

764

765 Chalmers, J.A. (1991) New evidence on the structure of the Labrador Sea/Greenland
766 continental margin. *J. Geol. Soc.*, 148(5), 899–908.

767

768 Chalmers, J.A. (1997) The continental margin off southern Greenland: along-strike
769 transition from an amagmatic to a volcanic margin. *J. Geol. Soc.*, 154(3), 571–576.

770

771 Chalmers, J.A. & Laursen, K.H. (1995) Labrador Sea: the extent of continental and
772 oceanic crust and the timing of the onset of seafloor spreading. *Mar. Pet. Geol.*, 12(2),
773 205–217.

774 Chalmers, J.A. & Pulvertaft, T.C.R. (2001) Development of the continental margins
775 of the Labrador Sea: a review. *Geol. Soc. London Spec. Publ.*, 187(1), 77–105.

776

777 Chattopadhyay, A. & Chakra, M. (2013) Influence of pre-existing pervasive fabrics
778 on fault patterns during orthogonal and oblique rifting: an experimental approach.
779 *Mar. Pet. Geol.*, 39(1), 74–91.

780

781 Chenin, P., Manatschal, G., Lavier, L.L. & Erratt, D. (2015) Assessing the impact of
782 orogenic inheritance on the architecture, timing and magmatic budget of the North
783 Atlantic rift system: a mapping approach. *J. Geol. Soc.*, 172, 711–720.

784

785 Chian, D., Keen, C., Reid, I. & Louden, K.E. (1995) Evolution of nonvolcanic rifted
786 margins: new results from the conjugate margins of the Labrador Sea. *Geology*, 23(7),
787 589–592.
788

789 Corti, G., van Wijk, J., Cloetingh, S. & Morley, C.K. (2007) Tectonic inheritance and
790 continental rift architecture: numerical and analogue models of the East African Rift
791 system. *Tectonics*, 26(6), 1–13.
792

793 Dalhoff, F., Chalmers, J.A., Gregersen, U., Nøhr-Hansen, H., Rasmussen, J.A. &
794 Sheldon, E. (2003) Mapping and facies analysis of Paleocene-Mid-Eocene seismic
795 sequences, offshore southern West Greenland. *Mar. Pet. Geol.*, 20(9), 935–986.
796

797 Dalhoff, F., Larsen, L.M., Ineson, J.R., Stouge, S., Bojesen-Koefoed, J.A., Lassen, S.,
798 Kuijpers, A., Rasmussen, J.A. & Nøhr-Hansen, H. (2006) Continental crust in the
799 Davis Strait: new evidence from seabed sampling. *Geol. Survey Denmark Greenland*
800 *Bulletin*, 10, 33–36.
801

802 De Paola, N., Holdsworth, R.E. & McCaffrey, K.J.W. (2005) The influence of
803 lithology and pre-existing structures on reservoir-scale faulting patterns in
804 transtensional rift zones. *J. Geol. Soc.*, 162, 471–480.
805

806 Dore, A.G., Lundin, E.R., Fichler, C. & Olesen, O. (1997) Patterns of basement
807 structure and reactivation along the NE Atlantic margin. *J. Geol. Soc.*, 154(1), 85–92.
808

809 Døssing, A. (2011) Fylla Bank: structure and evolution of a normal-to-shear rifted
810 margin in the northern Labrador Sea. *Geophys. J. Int.*, 187(2), 655–676.
811

812 Fjeldskaar, W., Helset, H.M., Johansen, H., Grunnaleite, I. & Horstad, I. (2008)
813 Thermal modelling of magmatic intrusions in the Gjallar Ridge, Norwegian Sea:
814 implications for vitrinite reflectance and hydrocarbon maturation. *Basin Res.*, 20,
815 143–159.
816

817 Funck, T., Jackson, H.R., Loudon, K.E. & Klingelhofer, F. (2007) Seismic study of
818 the transform-rifted margin in Davis Strait between Baffin Island (Canada) and

819 Greenland: what happens when a plume meets a transform. *J. Geophys. Res.: Solid*
820 *Earth*, 112(4), B04402.

821

822 Funck, T., Gohl, K., Damm, V. & Heyde, I. (2012) Tectonic evolution of southern
823 Baffin Bay and Davis Strait: results from a seismic refraction transect between
824 Canada and Greenland. *J. Geophys. Res.: Solid Earth*, 117(4), B04107.

825

826 Gibson, G.M., Totterdell, J.M., White, L.T., Mitchell, C.H., Stacey, A.R., Morse,
827 M.P. & Whitaker, A. (2013) Pre-existing basement structure and its influence on
828 continental rifting and fracture zone development along Australia's southern rifted
829 margin. *J. Geol. Soc.*, 170(2), 365–377.

830

831 Gregersen, U. & Skaarup, N. (2007) A mid-Cretaceous prograding sedimentary
832 complex in the Sisimiut Basin, offshore West Greenland-stratigraphy and
833 hydrocarbon potential. *Mar. Pet. Geol.*, 24(1), 15–28.

834

835 Grocott, J. & McCaffrey, K. (2017) Basin evolution and destruction in an early
836 Proterozoic continental margin: the Rinkian fold-thrust Belt of Central West
837 Greenland. *J. Geol. Soc.*, <https://doi.org/10.1144/jgs2016-109>.

838

839 Holdsworth, R.E., Butler, C.A. & Roberts, A.M. (1997) The recognition of
840 reactivation during continental deformation. *J. Geol. Soc.*, 154(1), 73–78.

841

842 Holdsworth, R.E., Handa, M., Miller, J.A. & Buick, I.S. (2001) Continental
843 reactivation and reworking: an introduction. *Geol. Soc. London Spec. Publ.*, 184(1),
844 1–12.

845

846 Houseman, G. & Molnar, P. (2001) Mechanisms of lithospheric rejuvenation
847 associated with continental orogeny. *Geol. Soc. London Spec. Publ.*, 184, 13–38.

848

849 Huerta, A. & Harry, D.L. (2012) Wilson cycles, tectonic inheritance, and rifting of the
850 North American Gulf of Mexico continental margin. *Geosphere*, 8(2), 374.

851

852 Japsen, P., Bonow, J.M., Peulvast, J.-P. & Wilson, R.W. (2006) Uplift, erosion and
853 fault reactivation in southern West Greenland. *GEUS Field Reports*, 63.

854 Keen, C.E., Dickie, K. & Dehler, S.A. (2012) The volcanic margins of the northern
855 Labrador Sea: insights to the rifting process. *Tectonics*, 31(1), 1–13.

856

857 Kerr, J.W. (1967) A submerged continental remnant beneath the Labrador Sea. *Earth*
858 *Planet. Sci. Lett.*, 2(4), 283–289.

859

860 Kerr, A., Hall, J., Wardle, R.J., Gower, C.F. & Ryan, B. (1997) New reflections on
861 the structure and evolution of the Makkovikian – Ketilidian Orogen in Labrador and
862 southern Greenland. *Tectonics*, 16(6), 942–965.

863

864 Koopmann, H., Brune, S., Franke, D. & Breuer, S. (2014) Linking rift propagation
865 barriers to excess magmatism at volcanic rifted margins. *Geology*, 42(12), 1071–
866 1074.

867

868 Korme, T., Acocella, V. & Abebe, B. (2004) The role of pre-existing structures in the
869 origin, propagation and architecture of faults in the main Ethiopian rift. *Gondwana*
870 *Res.*, 7(2), 467–479.

871

872 Korstgård, J., Ryan, B. & Wardle, R. (1987) The boundary between Proterozoic and
873 Archaean crustal blocks in central West Greenland and northern Labrador. *Geol. Soc.*
874 *London Spec. Publ.*, 27(1), 247–259.

875

876 Krabbendam, M. (2001) When the Wilson Cycle breaks down: how orogens can
877 produce strong lithosphere and inhibit their future reworking. *Geol. Soc. London*
878 *Spec. Publ.*, 184(1), 57–75.

879

880 Kuszniir, N.J. & Park, R.G. (1987) The extensional strength of the continental
881 lithosphere: its dependence on geothermal gradient, and crustal composition and
882 thickness. *Geol. Soc. London Spec. Publ.*, 28(1), 35–52.

883

884 Larsen, H.C. & Saunders, A.D. (1998) Tectonism and volcanism at the southeast
885 Greenland rifted margin: a record of plume impact and later continental rapture.

886 Proceedings of the Ocean Drilling Program, Scientific Results, 152,
887 <https://doi.org/10.2973/odp.proc.sr.152.1998>.

888

889 Larsen, L.M., Rex, D.C., Watt, W.S. & Guise, P.G. (1999) ^{40}Ar – ^{39}Ar dating of
890 alkali basaltic dykes along the south-west coast of Greenland: cretaceous and Tertiary
891 igneous activity along the eastern margin of the Labrador Sea. *Geol. Greenland*
892 *Survey Bulletin*, 184, 19–29.

893

894 Larsen, L.M., Heaman, L.M., Creaser, R.A., Duncan, R.A., Frei, R. & Hutchison, M.
895 (2009) Tectonomagmatic events during stretching and basin formation in the
896 Labrador Sea and the Davis Strait: evidence from age and composition of Mesozoic to
897 Palaeogene dyke swarms in West Greenland. *J. Geol. Soc.*, 166(6), 999–1012.

898

899 Lister, G.S., Etheridge, M.A. & Symonds, P.A. (1991) Detachment models for the
900 formation of passive continental margins. *Tectonics*, 10(5), 1038–1064.

901

902 Magee, C., Muirhead, J.D., Karvelas, A., Holford, S.P., Jackson, C.A.L., Bastow,
903 I.D., Schofield, N., Stevenson, C.T.E., McLean, C., McCarthy, W. & Shtukert, O.
904 (2016) Lateral magma flow in mafic sill complexes. *Geosphere*, 12(3), GES01256.

905

906 Magee, C., Jackson, C.A.-L., Hardman, J.P. & Reeve, M.T. (2017) Decoding sill
907 emplacement and forced fold growth in the Exmouth Sub-basin, offshore northwest
908 Australia: Implications for hydrocarbon exploration. *Interpretation*, 5(3), SK11–
909 SK22.

910

911 Manatschal, G., Lavier, L. & Chenin, P. (2015) The role of inheritance in structuring
912 hyperextended rift systems: some considerations based on observations and numerical
913 modeling. *Gondwana Res.*, 27(1), 140–164.

914

915 Manhica, A.D.S.T., Grantham, G.H., Armstrong, R.A., Guise, P.G. & Kruger, F.J.
916 (2001) Polyphase deformation and metamorphism at the Kalahari Craton —
917 Mozambique Belt boundary. *Geol. Soc. London Spec. Publ.*, 184(1), 303–322.

918

919 McGregor, E.D., Nielsen, S.B., Stephenson, R.A., Clausen, O.R., Petersen, K.D. &
920 Macdonald, D.I.M. (2012) Evolution of the west Greenland margin: offshore
921 thermostratigraphic data and modelling. *J. Geol. Soc.*, 169(5), 515–530.
922

923 McKenzie, D. (1978) Some remarks on the development of sedimentary basins. *Earth*
924 *Planet. Sci. Lett.*, 40(1), 25–32.
925

926 Morley, C.K., Haranya, C., Phoosongsee, W., Pongwapee, S., Kornsawan, A. &
927 Wonganan, N. (2004) Activation of rift oblique and rift parallel pre-existing fabrics
928 during extension and their effect on deformation style: examples from the rifts of
929 Thailand. *J. Struct. Geol.*, 26(10), 1803–1829.
930

931 Nøhr-Hansen, H. (2003) Dinoflagellate cyst stratigraphy of the Palaeogene strata
932 from the Hellefisk-1, Ikermiut-1, Kangâmiut-1, Nukik-1, Nukik-2 and Qulleq-1 wells,
933 offshore West Greenland. *Mar. Pet. Geol.*, 20(9), 987–1016.
934

935 Nutman, A.P. & Collerson, K.D. (1991) Very early Archean crustal-accretion
936 complexes preserved in the North Atlantic craton. *Geology*, 19(8), 791–794.
937

938 Oakey, G.N. & Chalmers, J. A. (2012) A new model for the Paleogene motion of
939 Greenland relative to North America : plate reconstructions of the Davis Strait and
940 Nares Strait regions between Canada and Greenland. *J. Geophys. Res.: Solid Earth*,
941 117 (B10), 1–28.
942

943 Peace, A., McCaffrey, K.J.W., Imber, J., Phethean, J., Nowell, G., Gerdes, K. &
944 Dempsey, E. (2016) An evaluation of Mesozoic rift-related magmatism on the
945 margins of the Labrador Sea: implications for rifting and passive margin asymmetry.
946 *Geosphere*, 12(6), 1701–1724.
947

948 Peace, A., McCaffrey, K., Imber, J., Hobbs, R., van Hunen, J. & Gerdes, K. (2017)
949 Quantifying the influence of sill intrusion on the thermal evolution of organic-rich
950 sedimentary rocks in nonvolcanic passive margins: an example from ODP 210-1276,
951 offshore Newfoundland, Canada. *Basin Res.*, 29(3), 249–265.
952

953 Petersen, K.D. & Schiffer, C. (2016) Wilson cycle passive margins: control of
954 orogenic inheritance on continental breakup. *Gondwana Res.*,
955 <https://doi.org/10.1016/j.gr.2016.06.012>.
956

957 Phillips, T.B., Jackson, C.A.-L., Bell, R.E., Duffy, O.B. & Fossen, H. (2016)
958 Reactivation of intrabasement structures during rifting: a case study from offshore
959 southern Norway. *J. Struct. Geol.*, 91, 54–73.
960

961 Piasecki, S. (2003) Neogene dinoflagellate cysts from Davis Strait, offshore West
962 Greenland. *Mar. Pet. Geol.*, 20(9), 1075–1088.
963

964 Polat, A., Wang, L. & Appel, P.W.U. (2014) A review of structural patterns and
965 melting processes in the Archean craton of West Greenland: evidence for crustal
966 growth at convergent plate margins as opposed to non-uniformitarian models.
967 *Tectonophysics*, 662, 67–94.
968

969 Rasmussen, J.A., Nøhr-Hansen, H. & Sheldon, E. (2003) Palaeoecology and
970 palaeoenvironments of the lower palaeogene succession, offshore West Greenland.
971 *Mar. Pet. Geol.*, 20(9), 1043–1073.

972 Rolle, F. (1985) Late Cretaceous – Tertiary sediments offshore central West
973 Greenland: Lithostratigraphy, sedimentary evolution, and petroleum potential. *Can.*
974 *J. Earth Sci.*, 22(7), 1001–1029.
975

976 Ryan, P.D. & Dewey, J.F. (1997) Continental eclogites and the Wilson Cycle. *J. Geol.*
977 *Soc.*, 154(3), 437–442.
978

979 Sandwell, D.T., Müller, R.D., Smith, W.H.F., Garcia, E. & Francis, R. (2014) New
980 global marine gravity model from CryoSat-2 and Jason-1 reveals buried tectonic
981 structure. *Science*, 346(6205), 65–67.
982

983 Schenk, C.J. (2011) Chapter 41 geology and petroleum potential of the West
984 Greenland-East Canada Province. *Arctic Petrol. Geol.*, 35 (1), 627–645.
985

986 Schiffer, C., Peace, A., Phethean, J., Gernigon, L., McCaffrey, K.J.W., Petersen, K.D.
987 & Foulger, G.R., (in press), The Jan Mayen Microplate complex and the Wilson
988 Cycle: in tectonic evolution: 50 Years of the Wilson Cycle concept. Geol. Soc.
989 London Spec. Publ.
990
991 Skogseid, J. (2001) Volcanic margins: geodynamic and exploration aspects. *Mar. Pet.*
992 *Geol.*, 18(4), 457–461.
993
994 Sørensen, A.B. (2006) Stratigraphy, structure and petroleum potential of the Lady
995 Franklin and Maniitsoq Basins, offshore southern West Greenland. *Petrol. Geosci.*,
996 12(3), 221–234.
997
998 Srivastava, S.P. (1978) Evolution of the Labrador Sea and its bearing on the early
999 evolution of the North Atlantic. *Geophys. J. Int.*, 52(2), 313–357.
1000
1001 St-Onge, M.R., Van Gool, J.A.M., Garde, A.A. & Scott, D.J. (2009) Correlation of
1002 Archaean and Palaeoproterozoic units between northeastern Canada and western
1003 Greenland: constraining the pre-collisional upper plate accretionary history of the
1004 Trans-Hudson orogen. *Geol. Soc. London Spec. Publ.*, 318(1), 193–235.
1005
1006 Storey, M., Duncan, R.A., Pedersen, A.K., Larsen, L.M. & Larsen, H.C. (1998)
1007 ⁴⁰Ar/³⁹Ar geochronology of the West Greenland Tertiary volcanic province. *Earth*
1008 *Planet. Sci. Lett.*, 160(3–4), 569–586.
1009
1010 Suckro, S.K., Gohl, K., Funck, T., Heyde, I., Ehrhardt, A., Schreckenberger, B.,
1011 Gerlings, J., Damm, V. & Jokat, W. (2012) The crustal structure of southern Baffin
1012 Bay: implications from a seismic refraction experiment. *Geophys. J. Int.*, 190(1), 37–
1013 58.
1014
1015 Suckro, S.K., Gohl, K., Funck, T., Heyde, I., Schreckenberger, B., Gerlings, J. &
1016 Damm, V. (2013) The Davis Strait crust-a transform margin between two oceanic
1017 basins. *Geophys. J. Int.*, 193(1), 78–97.
1018

1019 Tappe, S., Foley, S.F., Stracke, A., Romer, R.L., Kjarsgaard, B.A., Heaman, L.M. &
1020 Joyce, N. (2007) Craton reactivation on the Labrador Sea margins: $^{40}\text{Ar}/^{39}\text{Ar}$ age
1021 and Sr-Nd-Hf-Pb isotope constraints from alkaline and carbonatite intrusives. *Earth*
1022 *Planet. Sci. Lett.*, 256(3–4), 433–454.
1023

1024 Theunissen, K., Klerkx, J., Melnikov, A. & Mruma, A.H. (1996) Mechanisms of
1025 inheritance of rift faulting in the western branch of the East African Rift, Tanzania.
1026 *Tectonics*, 15(4), 776–790.
1027

1028 Thomas, W.A., Ravelo, A.C., Dekens, P.S. & McCarthy, M.D. (2006) Tectonic
1029 inheritance at a continental margin. *GSA Today*, 16(3), 4–11.
1030

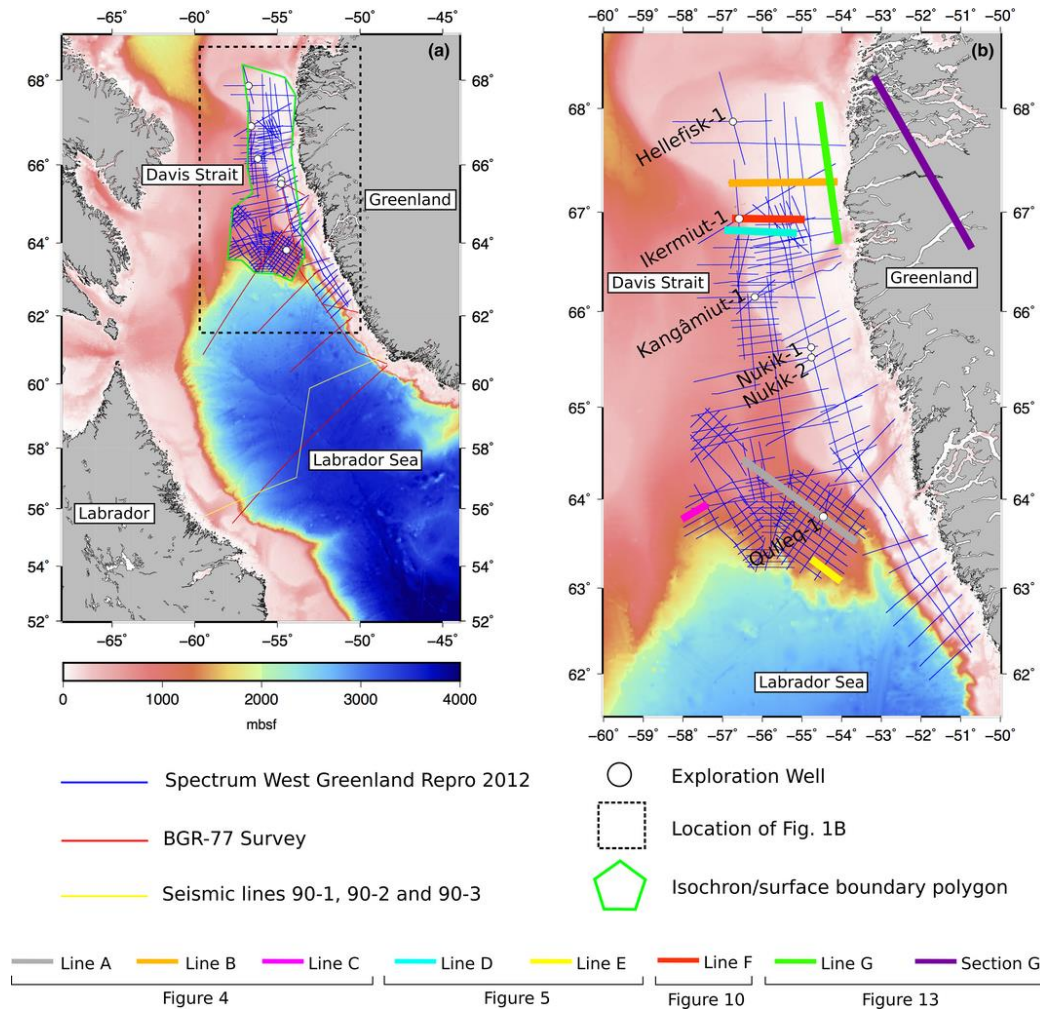
1031 Umpleby, D.C. (1979) Geology of the Labrador shelf. *Geol. Survey Canada*, 79–13.
1032

1033 Van Gool, J.A.M., Connelly, J.N., Marker, M. & Mengel, F.C. (2002) The
1034 Nagssugtoqidian Orogen of West Greenland: tectonic evolution and regional
1035 correlations from a West Greenland perspective. *Can. J. Earth Sci.*, 39(5), 665–686.
1036

1037 Wilson, T. (1966) Did the Atlantic close and the re-open? *Nature*, 209, 1246–1248.
1038

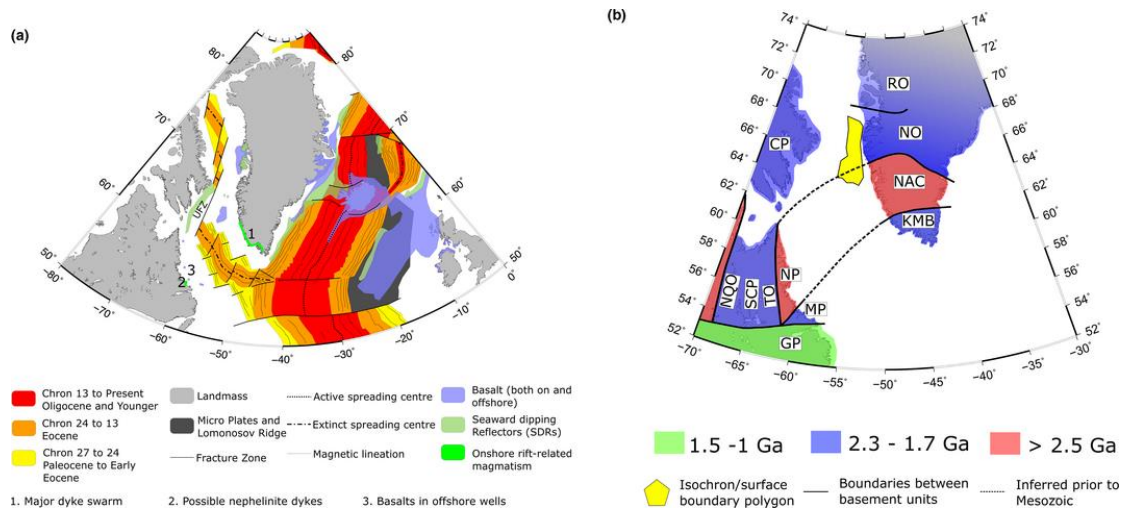
1039 Wilson, R.W., Klint, K.E.S., Van Gool, J.A.M., McCaffrey, K.J.W., Holdsworth, R.E.
1040 & Chalmers, J.A. (2006) Faults and fractures in central West Greenland: onshore
1041 expression of continental break-up and sea-floor spreading in the Labrador–Baffin
1042 Bay Sea. *Geol. Survey Denmark Greenland Bulletin*, 11, 185–204.
1043

1044 Wu, L., Trudgill, B.D. & Kluth, C.F. (2016) Salt diapir reactivation and normal
1045 faulting in an oblique extensional system, Vulcan Sub-basin, NW Australia. *J. Geol.*
1046 *Soc.*, 173, <https://doi.org/10.1144/jgs2016-008>.
1047



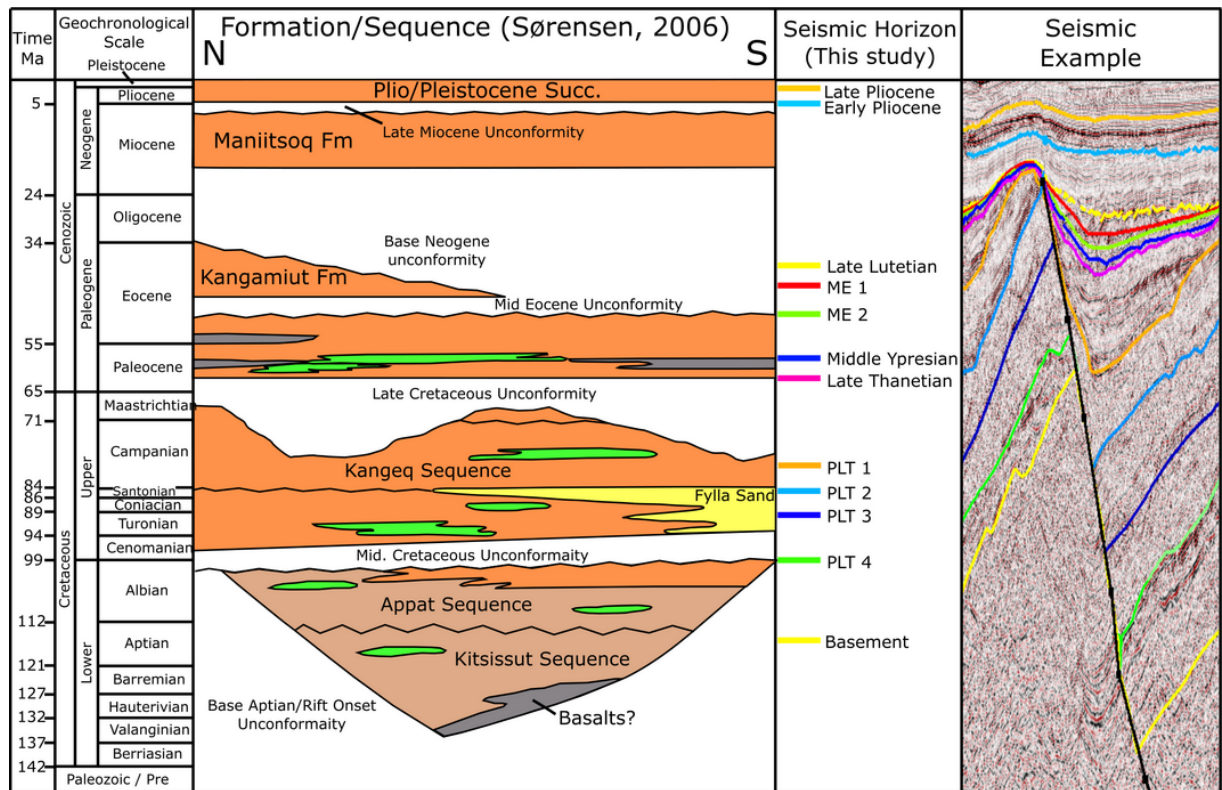
1049

1050 Figure 1. (a) The study area to the north of the Labrador Sea including: the
 1051 locations of the seismic datasets, the polygon used for surface and isochron
 1052 generation and the locations of the six exploration wells. (b) The study area
 1053 within the eastern Davis Strait including the names of the six exploration wells in
 1054 addition to the approximate locations of the seismic lines and geological cross
 1055 section displayed in this contribution. Both (a) and (b) are plotted using the
 1056 bathymetry data from Smith and Sandwell v17.1.
 1057



1058

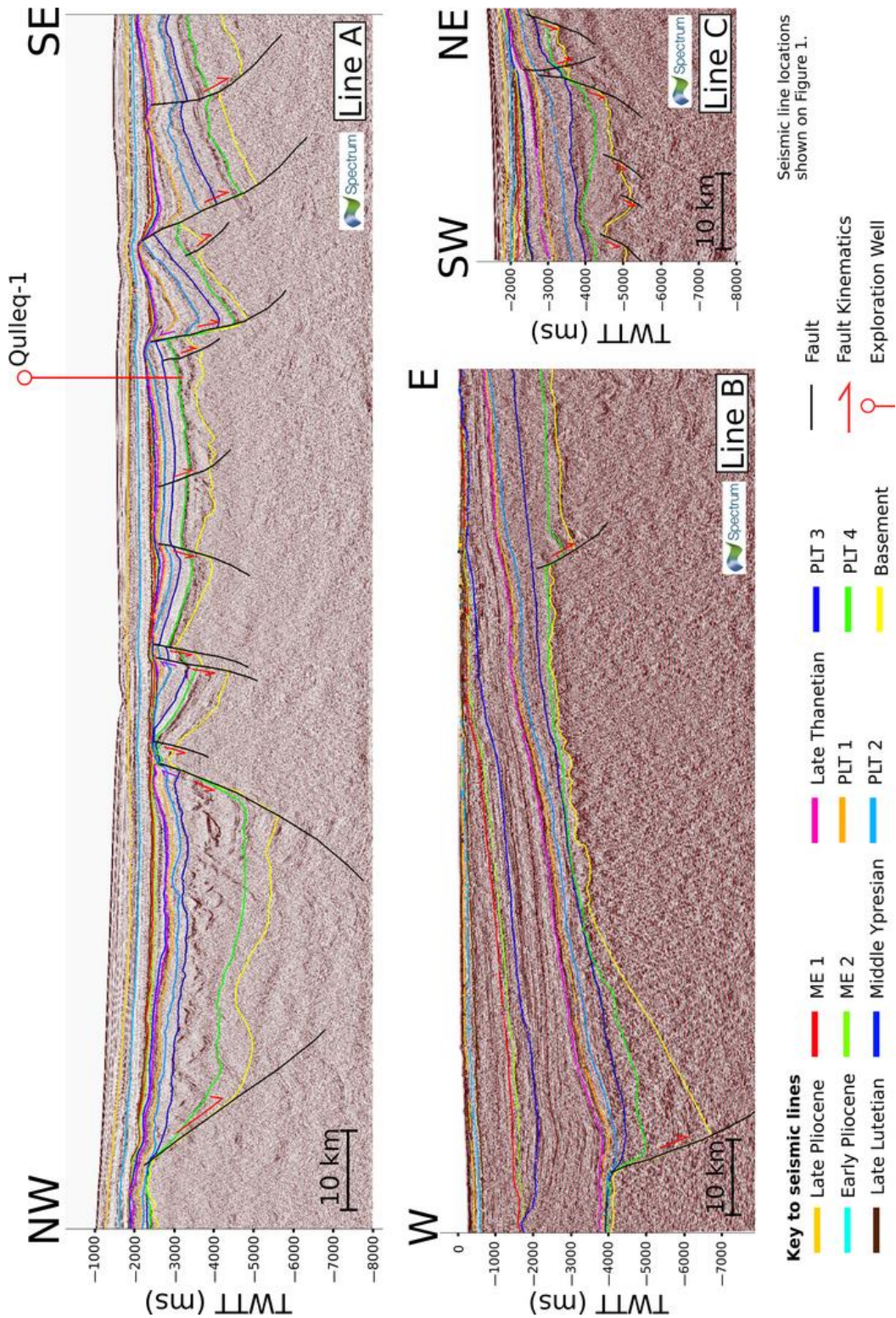
1059 Figure 2. (a) An overview of the North Atlantic oceanic spreading systems,
 1060 including: the age of oceanic crust; major active and extinct spreading axes;
 1061 major oceanic fracture zones; proposed microplates and magnetic lineations
 1062 (Oakey & Chalmers, 2012). The spatial distribution of onshore and offshore flood
 1063 basalts and seaward dipping reflectors (SDRs) are overlain (Larsen & Saunders,
 1064 1998) in addition to the magmatism in the Labrador sea-Baffin Bay rift system
 1065 described in previous work (Umpleby, 1979; Tappe *et al.*, 2007; Larsen *et al.*,
 1066 2009; Peace *et al.*, 2016). (b) The primary study area (yellow polygon) within a
 1067 simplified overview of basement units in north-eastern Canada and Greenland
 1068 modified from Kerr *et al.* (1997) and Van Gool *et al.* (2002). RO, Rinkian Orogen;
 1069 NO, Nagssugtoqidian; CP, Churchill Province; NQO, New Quebec Orogen; SCP,
 1070 Southern Churchill Province; TO, Torngat Orogen; NP, Nain Province; MP,
 1071 Makkovik Province; GP, Grenville Province; NAC, North Atlantic Craton; KMB,
 1072 Ketilidian Mobile Belt.
 1073



1074

1075 Figure 3. Stratigraphic framework for the study area (Fig. 1) modified from
 1076 Sørensen (2006) to include the stratigraphic locations of the horizons
 1077 interpreted in this study and an example seismic section.

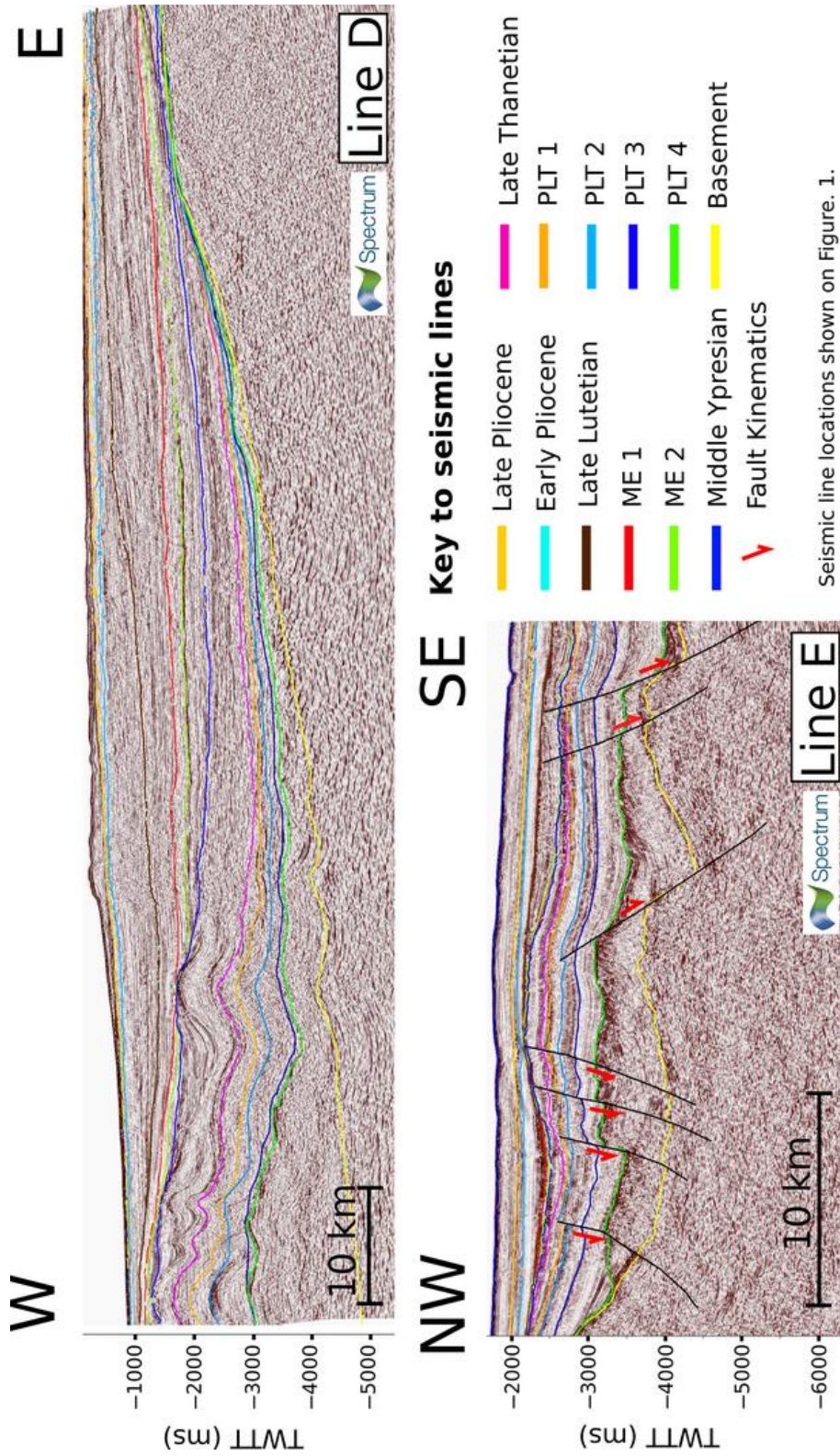
1078



1079

1080 Figure 4. Representative seismic reflection profiles from across the study area
 1081 (Fig. 1b). Line A is a NW-SE oriented seismic line from the southeast of the study
 1082 area, Line B is a W-E trending seismic line from the north of the study area and
 1083 Line C is a NE-SW trending seismic line from the southwest of the study area.

1084



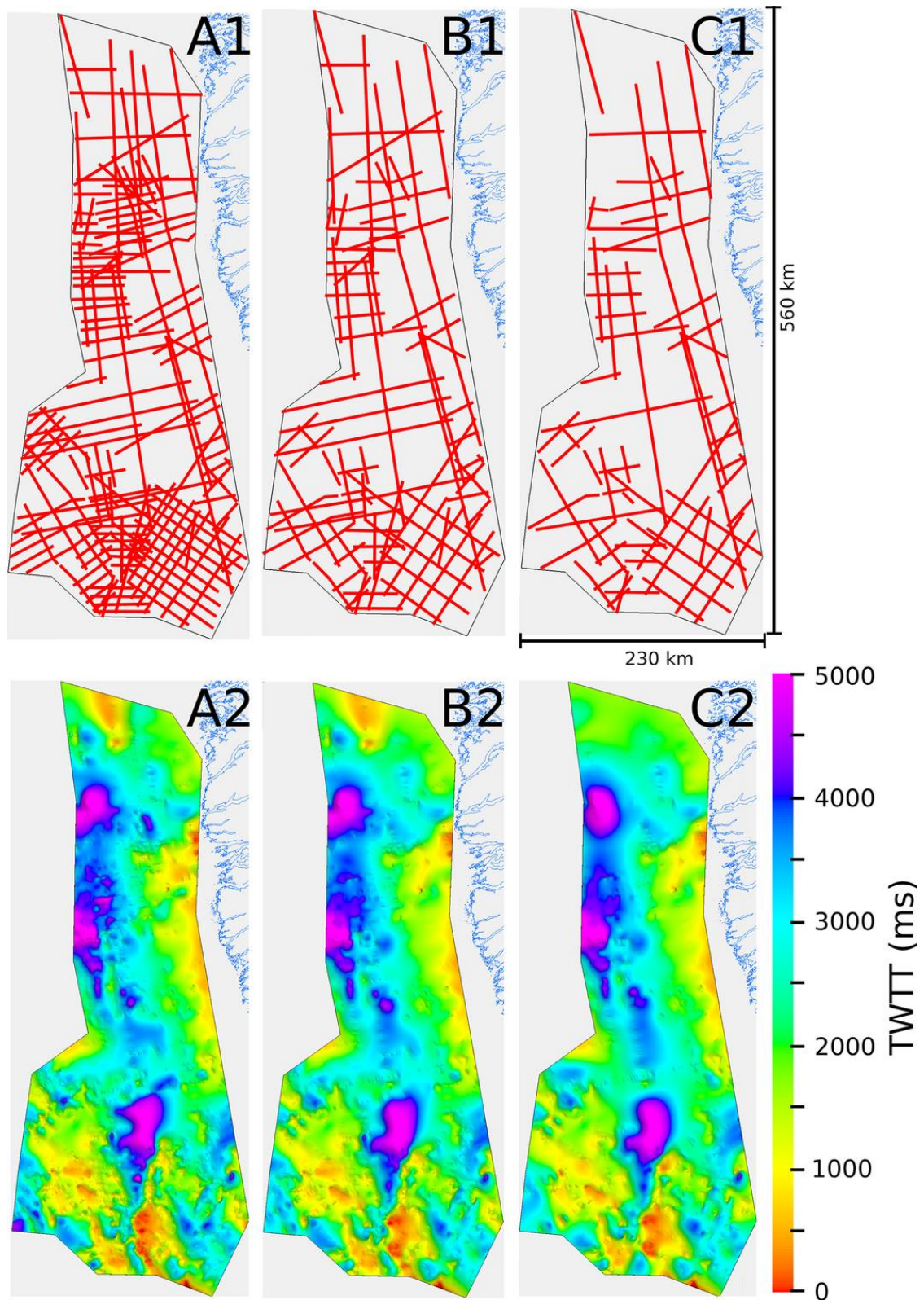
Seismic line locations shown on Figure. 1.

1086

1087 Figure 5. Line D is a W-E trending seismic line from the north of the study area

1088 and Line E is a NW-SE oriented seismic line from the south of the study area.

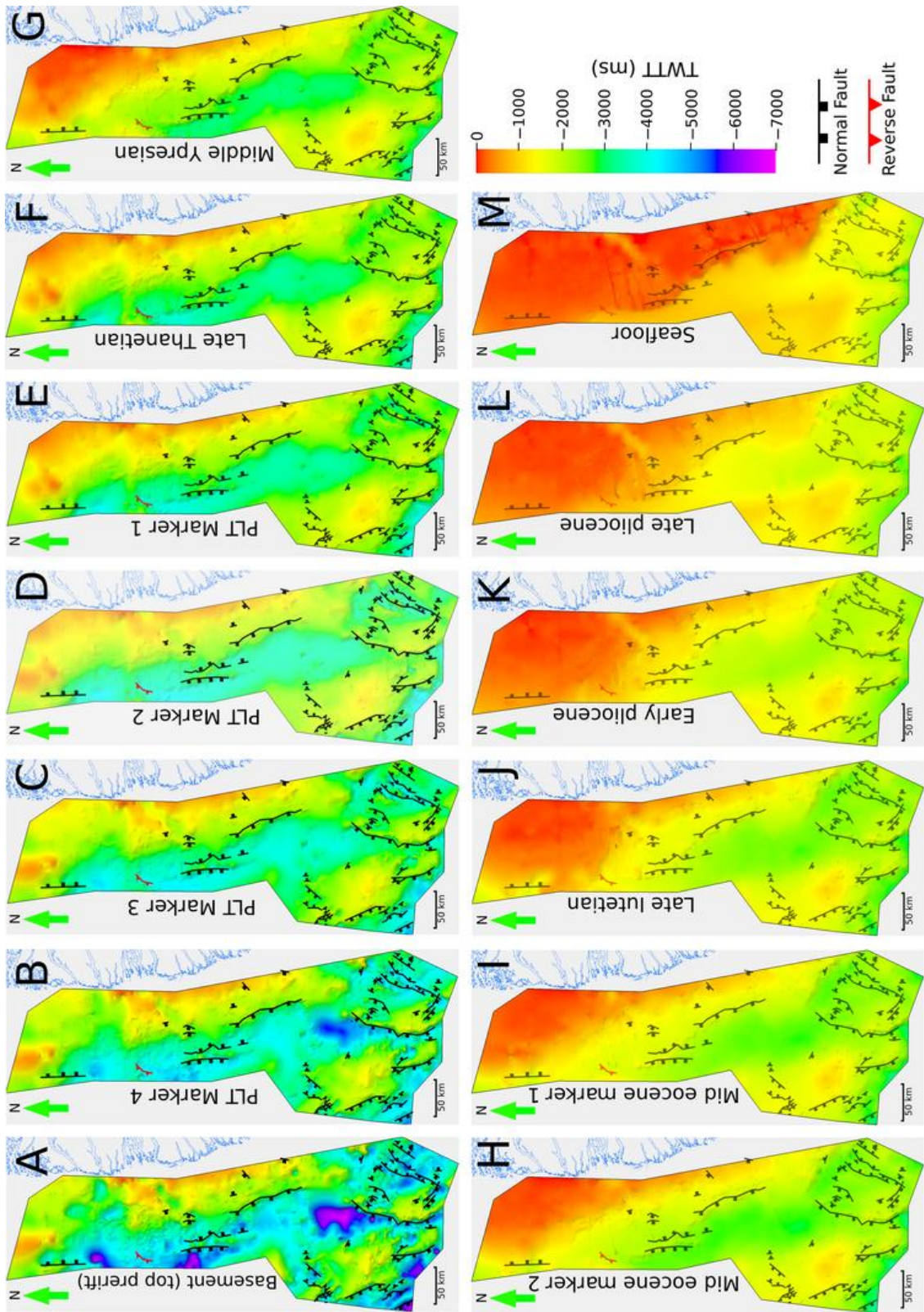
1089



1090

1091 Figure 6. Total sediment thickness (top basement horizon to seabed) maps
 1092 produced after thinning the seismic grid. The seismic grid above each isochron
 1093 depicts the lines used to produce the isochron below.

1094

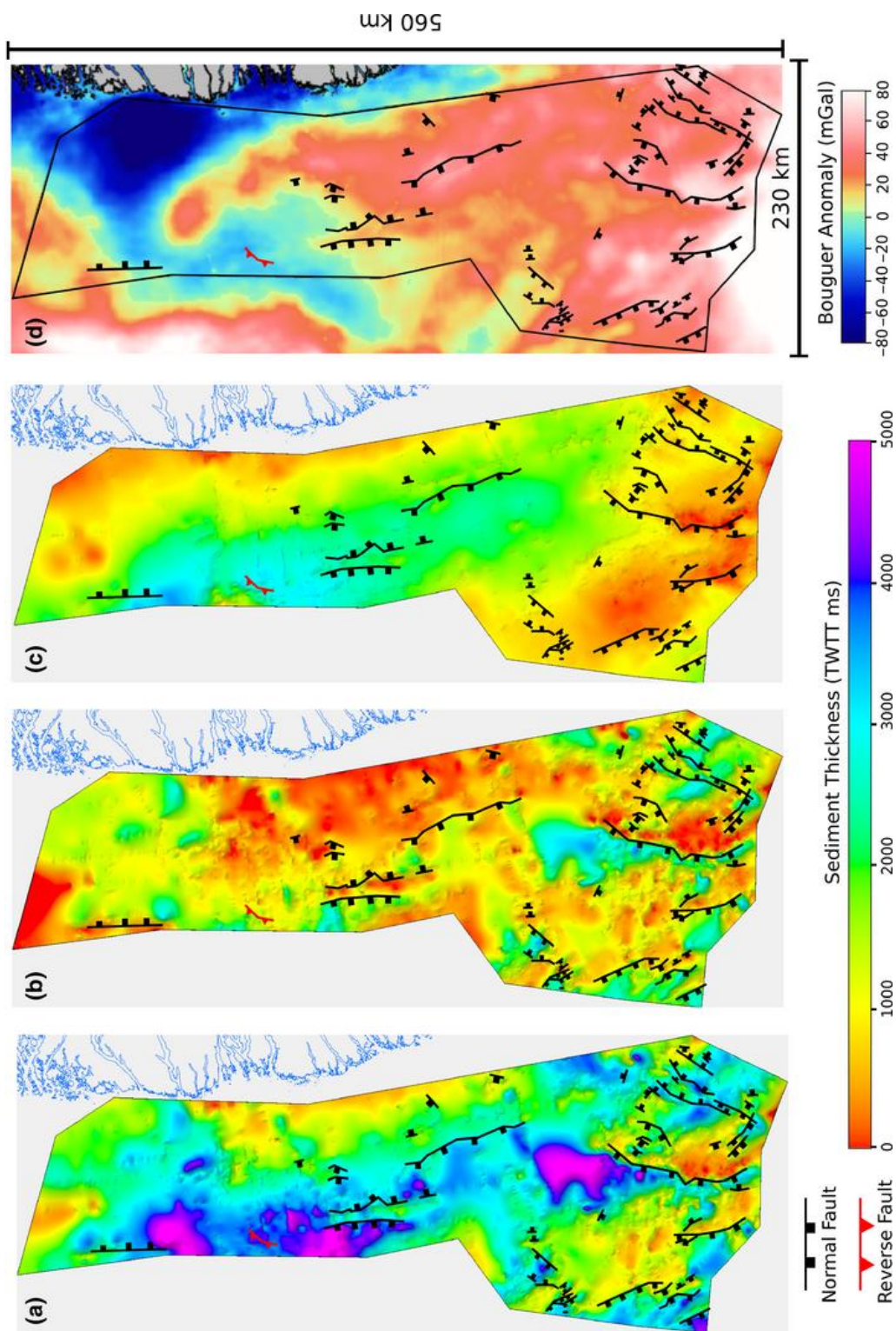


1095

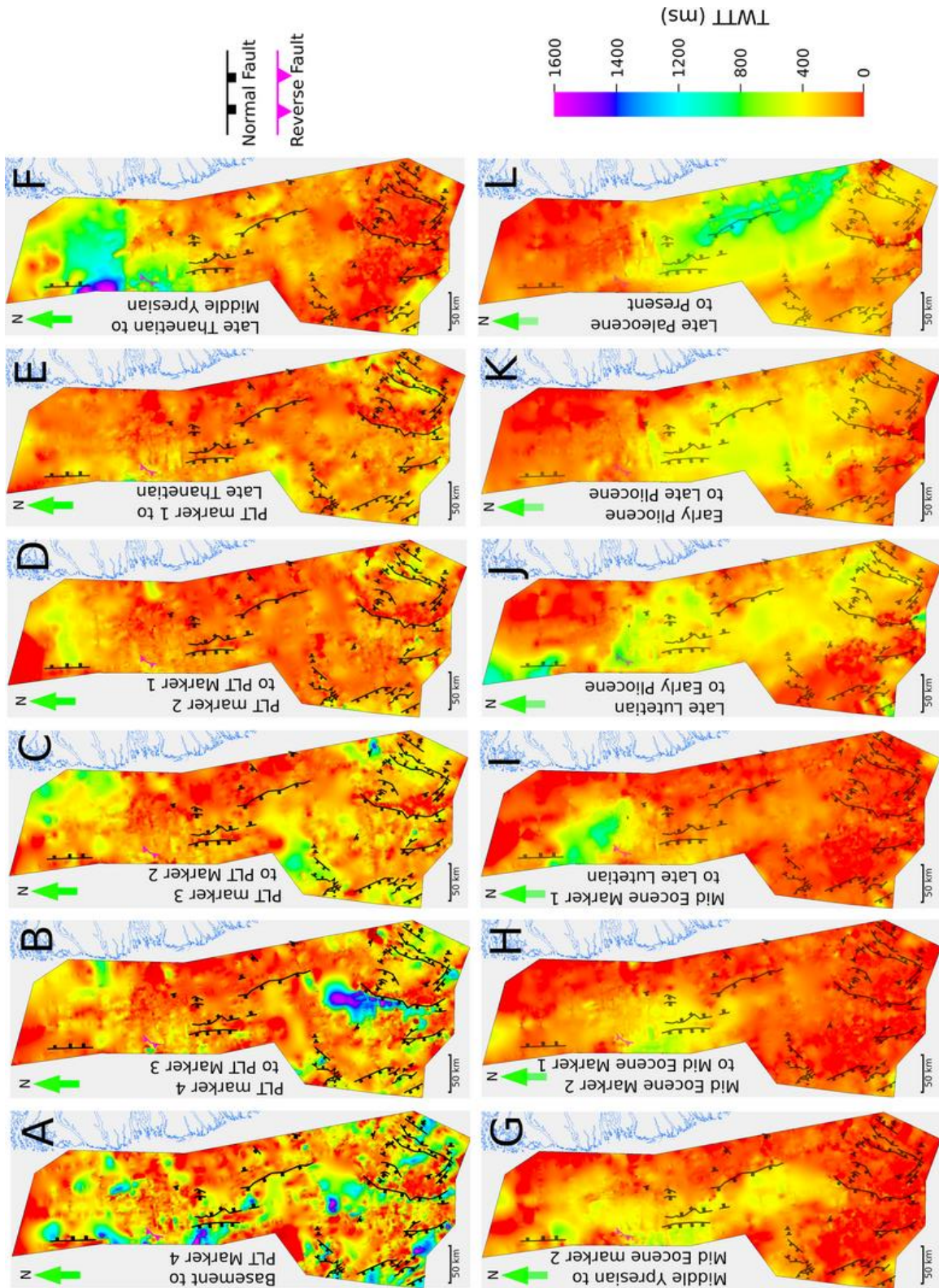
1096 Figure 7. Surfaces generated from each interpreted horizon, along with the
 1097 interpreted faults with transparency increasing through time to indicate the
 1098 diminishing role of such structures. PLT, Pre-Late Thanetian.

1099

1100



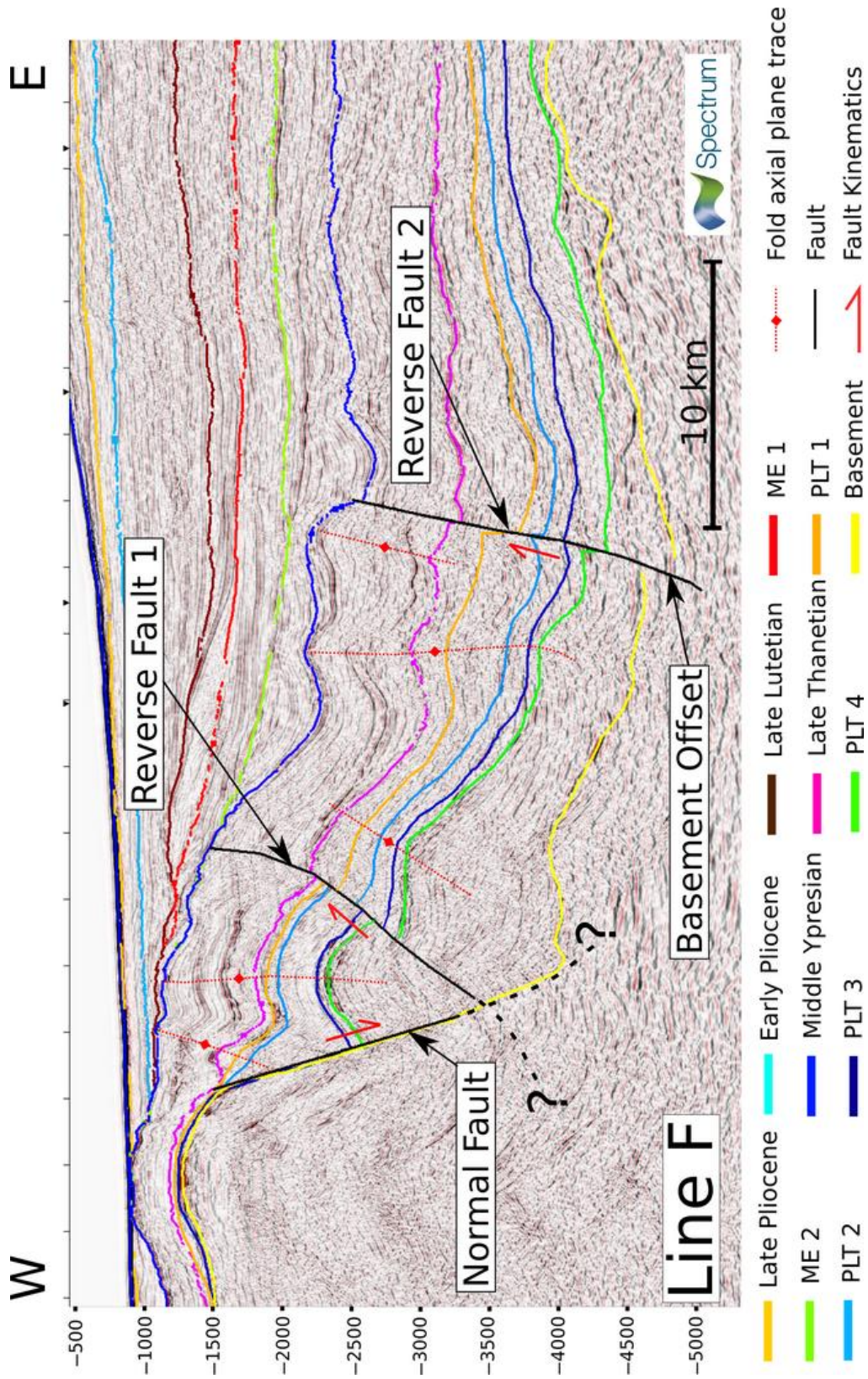
1101 Figure 8. Time thickness isochrons for: (a) Total sediment thickness, (b)
1102 Basement to Late Thanetian and (c) Late Thanetian to Seafloor (all in TWTT ms).
1103 (d) The Bouguer gravity anomaly calculated using Smith and Sandwell free air
1104 anomaly v23.1 by assuming an average crustal density of 2.7 g cm^{-3} . Also shown
1105 are the faults interpreted during this study.

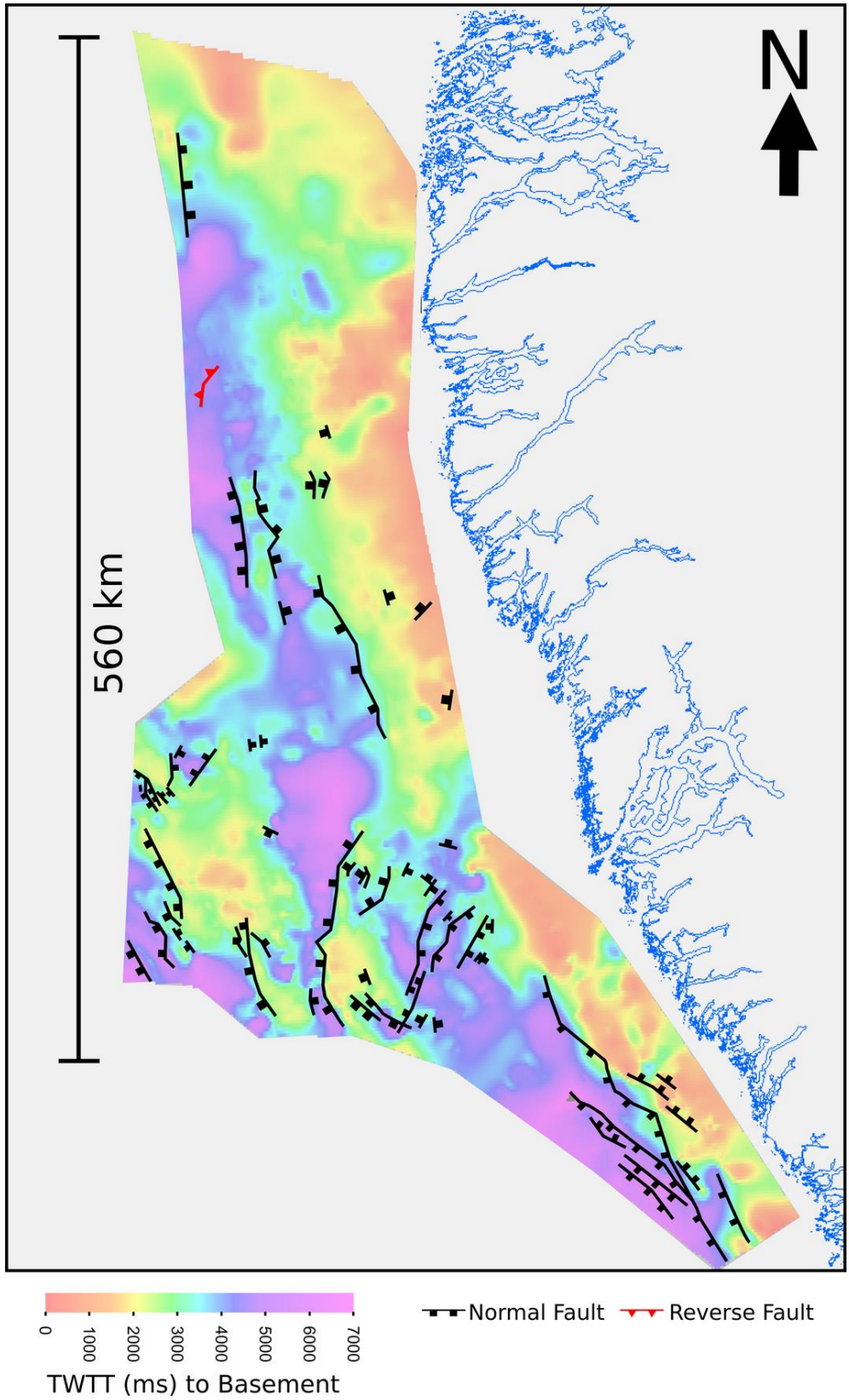


1106

1107 Figure 9. Isochrons for the defined geological intervals used in this study. Also
 1108 shown are the interpreted faults with transparency increasing through time to
 1109 indicate the diminishing role of such structures.

1110





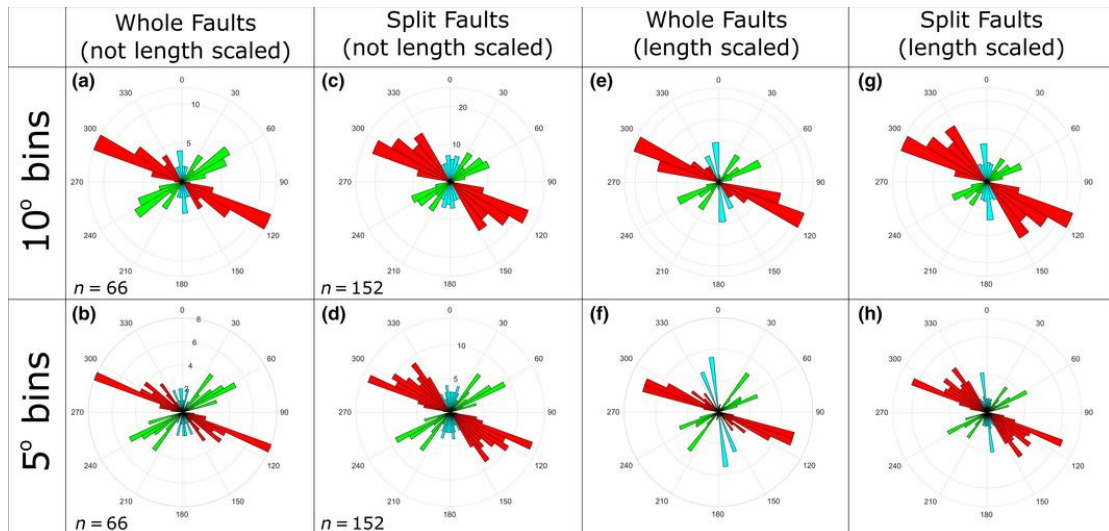
1115

TWTT (ms) to Basement

1116 Figure 11. Offshore fault map for the Eastern Davis Strait produced by this study

1117 overlain on the basement horizon in TWTT (ms).

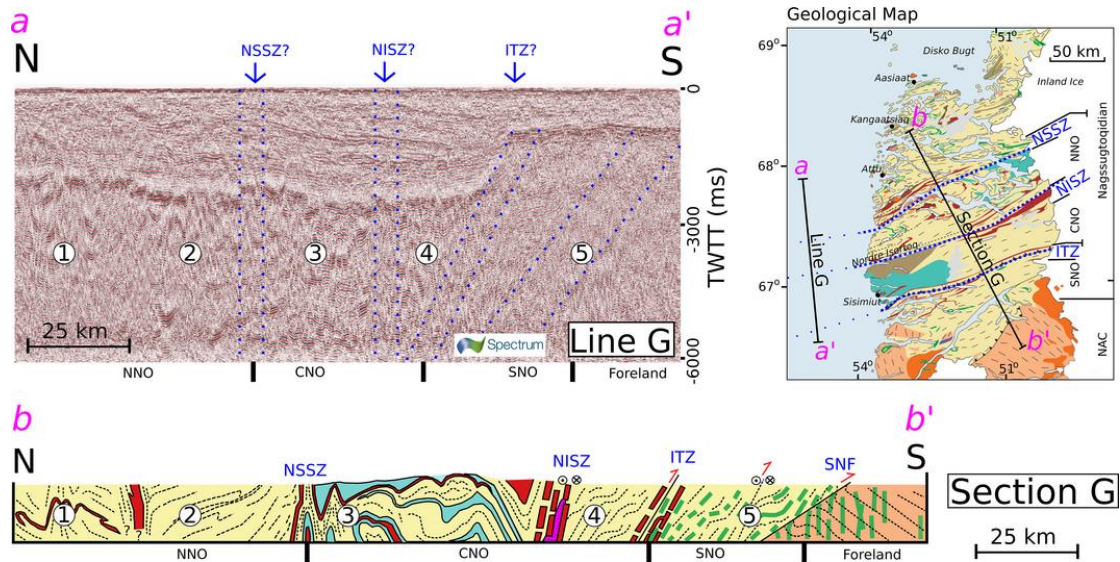
1118



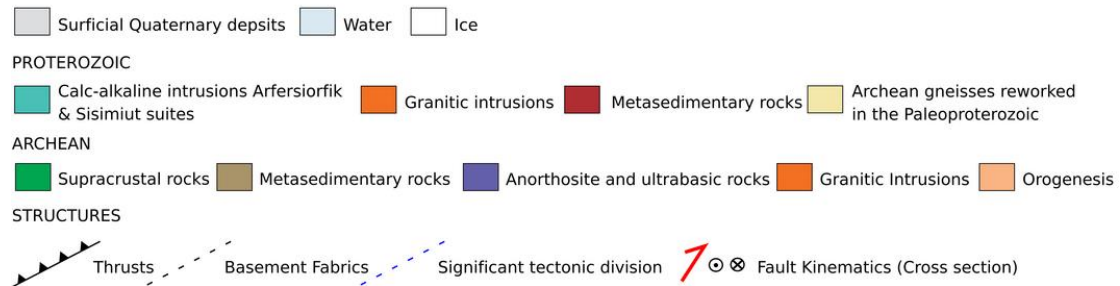
1119

1120 Figure 12. (a) Rose diagram for whole faults with 10° bins and not length scaled.
 1121 (b) Rose diagram for whole faults with 5° bins and not length scaled. (c) Rose
 1122 diagram for faults split at vertices with 10° bins and not length scaled. (d) Rose
 1123 diagram for faults split at vertices 5° bins and not length scaled. (e) Rose diagram
 1124 for whole faults with 10° bins and length scaled. (f) Rose diagram for whole
 1125 faults with 5° bins and length scaled. (g) Rose diagram for faults split at vertices
 1126 with 10° bins and length scaled. (h) Rose diagram for faults split at vertices 5°
 1127 bins and length scaled.

1128



Key to Seismic Line, Cross Section and Geological Map



1129

1130 Figure 13. Line G (a-a') is a N-S oriented seismic line from the northeast of the
 1131 study area that lies approximately adjacent to the onshore geological cross
 1132 section G (b-b'), as shown on the geological map insert on this figure. The
 1133 geological map and cross section of the Nagssugtoqidian orogen are modified
 1134 from Van Gool *et al.* (2002) and Wilson *et al.* (2006). NSSZ, Nordre Strømfjord
 1135 shear zone; NISZ, Nordre Isortoq shear zone; ITZ, Ikertôq thrust zone; NNO,
 1136 Northern Nagssugtoqidian orogeny; CNO, Central Nagssugtoqidian orogeny;
 1137 SNO, Southern Nagssugtoqidian orogeny; SNF, Southern Nagssugtoqidian front;
 1138 NAC, North Atlantic Craton.

1139

1153 **Tables**

Well Name	Latitude	Longitude	Date	TD (m)	TD Lithology/Formation
Hellefisk-1	67.877944	-56.739161	21/06/1977	3201.2	Basalt (Paleocene?)
Ikermiut-1	66.936572	-56.590681	12/07/1977	3619	Campanian shales
Kangamiut-1	66.150256	-56.190078	02/06/1976	3874	Precambrian basement
Nukik-1	65.526719	-54.760497	02/07/1977	2363.4	Precambrian basement
Nukik-2	65.631775	-54.766831	08/08/1977	2693.8	Mastrichtian Basalt
Qulleq-1	63.813342	-54.451836	10/07/2000	2973	Santonian Sandstones

1154 Table 1. Summary of exploration wells used in this study in the Davis Strait with the
1155 terminal depth (TD) in metres from the rotary table. Lithology at TD from Nøhr-
1156 Hansen (2003) and Rolle (1985).
1157

System No.	Ketilidian Mobile Belt (Japsen <i>et al.</i> 2006)			North Atlantic Craton (Japsen <i>et al.</i> 2006)				Nagssugtoqidian (Wilson <i>et al.</i> 2006)	This Study
	Landsat		Field	Landsat		Aerial	Field	Landsat, Aerial, Field	Seismic interpretation
	1:500,000	1:100,000		1:500,000	1:100,000				
1	NE-SW	No Dominant system. A range from NE-SW through to SE-NW.	N-S	N-S	N-S		N-S	ENE-WSW	NE-SW
2	N-S		NE- SW/ENE -WSW	NE-SW	NE-SW	NE-SW	NE- SW	N-S	NNW-SSE
3	NNW-SSE		E-W	ENE-WSW	ENE-WSW	ENE- WSW	ENE- WSW	NNW-SSE	NW-SE
4	NNE-SSW		ESE- WNW/ SE-NW	ESE-WNW	ESE-WNW		NW- SE	NNE-SSW	
5	E-W to ESE- WNW							E-W to ESE- WNW	

1158 Table 2. Summary of the onshore structural systems identified using different
1159 methodologies in the Ketilidian Mobile Belt, the North Atlantic Craton (Japsen *et al.*,
1160 2006) and the Nagssugtoqidian by Wilson *et al.* (2006) and Japsen *et al.* (2006).
1161 Orientations quoted in this table represent the strike of the feature.